Molecular models for the hydrogen age: Hydrogen, nitrogen, oxygen, argon and water

Andreas Köster,[†] Monika Thol,[‡] and Jadran Vrabec[*,†]

[†]*Lehrstuhl für Thermodynamik und Energietechnik, Universität Paderborn, 33098 Paderborn, Germany*

[‡]*Lehrstuhl für Thermodynamik, Ruhr-Universität Bochum, 44801 Bochum, Germany*

E-mail: jadran.vrabec@upb.de

Phone: +49-5251 60-2421. Fax: +49 5251 60-3522

Abstract

Thermodynamic properties including the phase behavior of all mixtures containing hydrogen, the main components of air, i.e. nitrogen, oxygen and argon, and water are of particular interest for the upcoming post-carbon age. Molecular modeling and simulation, the PC-SAFT equation of state as well as sophisticated empirical equations of state are employed to study the mixture behavior of these five substances. For this purpose, a new force field for hydrogen is developed. All relevant subsystems, i.e. binary, ternary and quaternary mixtures, are considered. The quality of the results is assessed by comparing to available experimental literature data, showing an excellent agreement in many cases. Molecular simulation, which is the most versatile approach in general, also provides the best overall agreement. Consequently, this contribution aims at an improved availability of thermodynamic data that are required for the hydrogen age.

Keywords

Hydrogen age, Molecular modeling and simulation, Equation of state, PC-SAFT

1 Introduction

Even in the international political arena, it is now globally accepted that human civilization must switch from fossil to renewable energy sources because atmospheric pollution threatens our climate[1]. Much less attention is being paid in these discussions that fossil fuel resources were always also a potent driver of conflict basically from the onset of industrialization[2,3]. An attractive alternative energy carrier is hydrogen (H_2) that has major advantages over carbon-based fuels. H_2 can be used in all kinds of combustion processes and can reduce harmful carbon dioxide (CO_2) emissions to a minimum. An approach with an even wider impact, avoiding thermal energy that is associated with the Carnot limit, is the usage of fuel cells to directly convert chemical energy from H_2 with ambient air into electric energy and water. 1 kg H_2 contains 33.3 kWh of chemical energy, if the lower heating value of H_2 is employed. Modern electrolysers require an electricity input of 52 kWh/kg on average, which corresponds to an electrical efficiency of 64 %[4]. Since renewable energy sources, such as wind or solar energy, are fluctuating in nature and need to be balanced, their excess power may be employed for hydrogen production[5].

Very prominent devices using H_2 as a fuel both for combustion and for fuel cells were the NASA space shuttles[6]. However, the whole classical transportation sector could in general profit from fuel cells as Momirlan and Veziroglu[6] point out. In 2016, over 100 fuel cell buses for public transportation were in use worldwide[7]. More recently, first test runs with a new fuel cell passenger train were performed[8]. There are, however, numerous other meaningful approaches for the usage of H_2[9]. It may, e.g., be processed together with CO_2 in a power to gas approach and subsequently stored in the form of methane in widely available storage facilities[10]. All of these techniques have in common that accurate thermodynamic data are

needed for their design and optimization.

Since experimental measurements alone do not keep up with the demand for thermodynamic data, it must also be focused on other methods, which is the goal of this study. Accordingly, the mixture behavior of five substances related to the hydrogen age, i.e. H_2, nitrogen (N_2), oxygen (O_2), argon (Ar) and water (H_2O), is tackled with molecular modeling and simulation, the PC-SAFT equation of state (EOS) as well as sophisticated empirical EOS and compared to experimental data, if available. All relevant subsystems are described. Several literature studies already dealt with some of these subsystems. Stoll et al.[11] and Vrabec et al.[12] performed molecular simulation studies on binary mixtures related to dry air (N_2 + O_2, N_2 + Ar and Ar + O_2), which were then used to predict cryogenic vapor-liquid equilibria (VLE) of dry air (N_2 + O_2 + Ar)[13,14]. Furthermore, humid air (N_2 + O_2 + Ar + H_2O) was examined by Eckl et al.[14]. Related studies with a different objective, i.e. CO_2 mixtures for carbon capture and sequestration (CCS) and the like, were conducted by means of molecular modeling and simulation by Vrabec et al.[15] (N_2 + O_2 + CO_2), Tenorio et al.[16] (H_2 + CO_2) and Cresswell et al.[17] (binary mixtures of CO_2 with H_2, N_2, Ar and O_2). Moreover, several studies employed the statistical associating fluid theory (SAFT) in its various forms or cubic EOS to study mixtures containing CO_2[18,19]. Solubilities of binary aqueous systems (N_2 + H_2O and H_2 + H_2O) were examined by Sun et al.[20] with the SAFT-Lennard-Jones EOS. Finally, empirical multiparameter EOS formulated in terms of the Helmholtz energy are available, namely the GERG-2008[21] and a recently developed model for combustion gases (EOS-CG)[22]. These EOS are typically very accurate in reproducing experimental data. However, the EOS-CG unfortunately does not cover H_2 and the GERG-2008 EOS does not aim at cryogenic conditions. Consequently, a comprehensive study focusing on carbon-free mixtures containing H_2 is a necessity.

Different thermodynamic properties were considered in this work to describe a substantial number of mixtures. Apart from VLE properties, like vapor pressure, saturated densities or residual enthalpy of vaporization, also homogeneous density and solubility were studied. Sol-

ubility, i.e. Henry's law constant, is typically relevant for mixtures in which one component is only little soluble in the other, as it is the case for aqueous systems that are considered in the present work. In the following sections, the employed models are described before the results of this study are presented and discussed. Finally, a conclusion sums the present work up.

2 Methodology

2.1 Modeling of pure fluids and mixtures

In this study, non-polarizable force fields were employed for the intermolecular interactions. Due to the small size of all considered molecules, the internal degrees of freedom were neglected throughout. Dispersive and repulsive interactions were described with the widely known Lennard-Jones (LJ) 12-6 potential, whereas electrostatic interactions, if present, were modeled with point charges or point quadrupoles. Under these assumptions, the total intermolecular potential writes as

$$U = \sum_{i=1}^{N-1} \sum_{j=i+1}^{N} \left\{ \sum_{a=1}^{S_i^{\mathrm{LJ}}} \sum_{b=1}^{S_j^{\mathrm{LJ}}} 4\varepsilon_{ijab} \left[\left(\frac{\sigma_{ijab}}{r_{ijab}} \right)^{12} - \left(\frac{\sigma_{ijab}}{r_{ijab}} \right)^{6} \right] + \right.$$
$$\left. \sum_{c=1}^{S_i^{\mathrm{e}}} \sum_{d=1}^{S_j^{\mathrm{e}}} \frac{1}{4\pi\varepsilon_0} \left[\frac{q_{ic} q_{jd}}{r_{ijcd}} + \frac{q_{ic} Q_{jd} + Q_{ic} q_{jd}}{r_{ijcd}^3} \cdot f_1\left(\boldsymbol{\omega}_i, \boldsymbol{\omega}_j\right) + \frac{Q_{ic} Q_{jd}}{r_{ijcd}^5} \cdot f_2\left(\boldsymbol{\omega}_i, \boldsymbol{\omega}_j\right) \right] \right\}. \tag{1}$$

Therein, the pairwise interaction between LJ site a on molecule i and LJ site b on molecule j with a mutual distance r_{ijab} is specified by the LJ energy parameter ε_{ijab} and the LJ size parameter σ_{ijab}. q_{ic}, Q_{ic}, q_{jd} and Q_{jd} represent the point charge magnitudes and quadrupolar moments of electrostatic interaction site c on molecule i and interaction site d on molecule j, respectively, while ε_0 denotes the permittivity of the vacuum. The orientational depen-

dence of the electrostatic interactions is considered through the trigonometric expressions $f_x(\boldsymbol{\omega}_i, \boldsymbol{\omega}_j)$[23]. Finally, the summation limits N, S_x^{LJ} and S_x^{e} denote the number of molecules, the number of LJ sites and the number of electrostatic sites, respectively.

The force fields for Ar, N_2 and O_2 were taken from the work of Vrabec et al.[24]. These force fields were adjusted to experimental VLE data and it was shown that they are an adequate choice for numerous fluid mixtures[17,25–28]. For H_2O, the widely appreciated TIP4P/2005 force field[29], which performs well for a large variety of thermodynamic properties[30–32], was employed.

The description of molecular hydrogen with semi-empirical force fields or other common thermodynamic models, like EOS, is challenging. Due to its small mass, quantum effects have to be taken into account. These effects have a strong influence on macroscopic thermodynamic properties, especially at low temperatures[33]. Therefore, a force field that was adjusted to the VLE properties of hydrogen at low temperatures will lead to poor results using classical atomistic simulations at higher temperatures. Furthermore, molecular hydrogen is anisotropic because of its two nuclei and its nonspherical charge distribution and typically consists of ortho and para hydrogen with different quantum spin states[34]. Several authors have been working on modeling H_2 in the last decades, describing the intermolecular interactions with a single LJ 12-6 site[35], a LJ 12-6 site with an additional point quadrupole for the anisotropic interactions[36–38], or more complex force fields, which also account for many-body polarization[39]. In this work, both a single site LJ force field, initially taken from Hirschfelder et al.[35] and subsequently adjusted to speed of sound and thermal (pVT) properties of H_2 at temperatures from 50 to 250 K, and one with an additional point quadrupole from Marx and Nielaba[36] were considered. All force field parameters are listed in Table 1. It should be noted that point quadrupoles can easily be represented with a set of three point charges if required[40].

When describing mixtures, interactions between unlike molecules have to be taken into account. The unlike dispersive and repulsive interactions between LJ site a of molecule i

Table 1: Parameters of the present molecular interaction force fields.

Interaction Site	x Å	y Å	σ Å	$\varepsilon/k_{\mathrm{B}}$ K	q e	Q DÅ
Hydrogen A						
H_2	0	0	3.0366	25.84		
Hydrogen B[36]						
H_2	0	0	2.9580	36.7		0.6369
Nitrogen[24]						
N	0	-0.5232	3.3211	34.897		
N	0	0.5232	3.3211	34.897		
Quadrupole	0	0				-1.4397[1]
Oxygen[24]						
O	0	-0.4850	3.1062	43.183		
O	0	0.4850	3.1062	43.183		
Quadrupole	0	0				-0.8081[1]
Argon[24]						
Ar	0	0	3.3952	116.79		
Water[29]						
O	0	0	3.1589	93.2		
H	0.5859	0.7570			0.5564	
H	0.5859	-0.7570			0.5564	
M (Mid Point)	0.1546	0			-1.1128	

[1] The quadrupole is oriented along the molecular axis.

and LJ site b of molecule j were specified with the modified Lorentz-Berthelot combination rule

$$\sigma_{ijab} = \frac{\sigma_{iiaa} + \sigma_{jjbb}}{2}, \tag{2}$$

and

$$\varepsilon_{ijab} = \xi(\varepsilon_{iiaa}\varepsilon_{jjbb})^{1/2}. \tag{3}$$

The temperature independent binary interaction parameter ξ was adjusted to achieve a better representation of experimental mixture data. This adjustment can most favorably be done on the basis of one experimental data point of the vapor pressure at an equimolar composition because the binary interaction parameter ξ has the strongest influence under these conditions[41]. If a binary interaction parameter is available, mixtures with more than two components do not require further optimization because of pairwise additivity. The unlike electrostatic interactions were treated straightforwardly according to the laws of electrostatics and do not require any binary interaction parameters.

2.2 Simulation details

Throughout, Monte Carlo (MC) sampling[42] with the release 3.0 of the molecular simulation program *ms2*[43–45] was used to generate the thermodynamic data presented here. A cutoff radius of 15 Å was employed. The LJ long-range corrections, considering the interactions beyond the cutoff radius, were calculated with the angle-averaging method of Lustig[46], whereas long-range electrostatic interactions were considered by means of the reaction field method[23]. Statistical uncertainties of the simulation data were estimated by averaging over a sufficiently large number of uncorrelated blocks consisting of 5000 MC cycles each[47]. Three different molecular simulation workflows were employed:

1. VLE calculations were carried out with the grand equilibrium method[48]. This approach consists of two independent and subsequent simulation runs for the two phases in equilibrium. For the liquid phase, 864 particles were sufficiently equilibrated and then

sampled for 10^6 production cycles in the isobaric-isothermal (NpT) ensemble. One such cycle consists of $M/3 \cdot 864$ translational and rotational as well as one volume move attempt, where M is the number of molecular degrees of freedom. The chemical potential of every component in the liquid phase was sampled with Widom's test particle insertion[49]. From the results of this run, the chemical potential as a function of pressure $\mu_i(p)$ at constant liquid composition was approximated by a Taylor series expansion. This function was used in the subsequent pseudo grand canonical (μVT) ensemble simulation of the vapor phase to sample the vapor pressure. For this run 1000 particles were used, which were thoroughly equilibrated in advance. The production phase was $2 \cdot 10^5$ MC cycles, which consisted of $M/3 \cdot 1000$ particle displacements as well as three insertion and three deletion attempts. More details on the grand equilibrium method can be found elsewhere[48].

2. The Henry's law constant H_i was sampled in the NpT ensemble in the saturated liquid state of the solvent, i.e. H_2O, using 1000 particles. H_i is closely related to the chemical potential at infinite dilution μ_i^∞[50]

$$H_i = \rho_s k_B T \exp(\mu_i^\infty / (k_B T)), \tag{4}$$

wherein ρ_s is the saturated liquid density of the solvent, T the temperature and k_B Boltzmann's constant. The chemical potential at infinite dilution was obtained with Widom's test particle insertion[49]. For this purpose, the mole fraction of the solute was set to zero such that only test particles were inserted into the pure solvent. The simulation runs consisted of $3 \cdot 10^6$ MC cycles, i.e. $2 \cdot 10^5$ equilibration and $2.8 \cdot 10^6$ production cycles.

3. pVT calculations for homogeneous bulk phases were carried out in the NpT ensemble using 864 particles. After a thorough equilibration, the density ρ was sampled over 10^6 production cycles. Again, one cycle consisted of $M/3 \cdot 864$ translational and rotational

as well as one volume move attempt.

2.3 PC-SAFT equation of state

In addition to atomistic molecular simulation, the perturbed-chain statistical associating fluid theory (PC-SAFT) EOS was employed. It is also based on theoretical considerations (i.e. intermolecular interactions) and can therefore, like atomistic molecular simulation, be used in cases where only little experimental data are available. Since Gross and Sadowski developed the PC-SAFT EOS in 2001[51], several improvements were implemented. Having only three pure component parameters in its initial form, Gross and Sadowski added a term to account for association in 2002 that requires two additional parameters[52]. Further developments involved e.g. Helmholtz energy contributions of polar interactions[53–55] or cross associations[56]. Numerous studies showed that the PC-SAFT EOS is a powerful predictive approach to mixture behavior[19,57,58].

Since pairwise additivity is assumed, modeling mixtures in the PC-SAFT framework is reduced to the description of unlike chain interactions. This was done here with the modified Lorentz-Berthelot combination rule, cf. Eqs. (2) and (3), with a slightly different expression for the unlike energy parameter

$$\varepsilon_{ij} = (1 - k_{ij})(\varepsilon_i \varepsilon_j)^{1/2}, \tag{5}$$

wherein k_{ij} is a temperature independent binary parameter.

The pure component parameters of the PC-SAFT EOS were taken from the literature[18,51,59,60], cf. Table 2. It has to be noted that H_2 is modeled as a spherical molecule having similar parameters as the force field developed in this work. VLE properties and homogeneous densities can be calculated straightforwardly with the PC-SAFT EOS. Solubilty data, i.e. the Henry's law constant, can be obtained with the PC-SAFT EOS through the fugacity coefficient of a solute at infinite dilution. This approach was, e.g., utilized by

Vinš and Hrubý[61] for the solubility of N_2 in refrigerants. Note that, these systems exhibit solubilities which are orders of magnitude larger than those of the present aqueous systems.

The solubility of H_2, N_2, O_2 and Ar in H_2O could not be reproduced satisfactorily with PC-SAFT EOS, applying even more complex methods. Various H_2O models with several association schemes (2B, 4C), permanent polarities for both H_2O and the solutes as well as induced association as described by Kleiner and Sadowski[56] led only to little improvement. Therefore, modeling the solubility of the present aqueous mixtures with the PC-SAFT EOS was omitted in the main body of this study. However, some solubility results from the PC-SAFT EOS are shown in the supporting information.

Table 2: Pure component parameters of the PC-SAFT EOS.

Component	M	m	σ	ε/k_B	$\kappa^{A_iB_i}$	$\varepsilon^{A_iB_i}/k_\mathrm{B}$
	g/mol	-	Å	K	-	K
Hydrogen[59]	2.016	1	2.9150	37.00	-	-
Nitrogen[51]	28.010	1.2053	3.3130	90.96	-	-
Oxygen[18]	32.050	1.1217	3.2100	114.96	-	-
Argon[51]	39.948	0.9285	3.4784	122.23	-	-
Water[60]	18.015	2.5472	2.1054	138.63	0.2912	1718.2

2.4 Peng-Robinson equation of state

Empirical EOS are typically used to correlate thermodynamic data from experiment, offering inter- and extrapolation capabilities between and beyond these data. Being simple and often considered to be accurate enough to cover a wide range of thermodynamic properties, the Peng-Robinson EOS[62] is one of the most widely used cubic EOS[63]. It is given by

$$p = \frac{RT}{v-b} - \frac{a(T)}{v(v+b)+b(v-b)}, \tag{6}$$

with pressure p, universal gas constant R, molar volume v and two substance-specific parameters

$$a(T) = 0.45724 \frac{(RT_\mathrm{c})^2}{p_\mathrm{c}} \alpha(T), \tag{7}$$

and

$$b = 0.07780 \frac{RT_\mathrm{c}}{p_\mathrm{c}}. \tag{8}$$

Therein, T_c and p_c are the critical temperature and pressure. Numerous alpha functions $\alpha(T)$ were proposed in the literature, e.g. by Soave[64], Peng and Robinson[62], Mathias and Copeman[65] or Stryjek and Vera[66]. However, the best overall results for the present fluid mixtures were achieved here with the alpha function of Twu et al.[67]

$$\alpha = (T/T_c)^{N(M-1)} \exp(L(1 - (T/T_c)^{NM})), \tag{9}$$

wherein L, M and N are substance-specific parameters, which are usually fitted to pure component vapor pressure data. Table 3 lists the numerical values for L, M and N for the pure substances considered in the present work[68].

Table 3: Pure component parameters of the Twu-Bluck-Cunningham-Coon alpha function according to the Dortmund data base[68].

Component	T_c	p_c	L	M	N
	K	MPa	-	-	-
Hydrogen	33.2	1.297	0.926823	5.127460	0.084639
Nitrogen	126.2	3.394	0.329500	0.882750	1.052080
Oxygen	154.6	5.046	0.550161	0.933432	0.693063
Argon	150.8	4.874	0.557990	0.998454	0.669817
Water	647.3	22.048	0.44132	0.87340	1.75990

Mixtures can be represented by applying mixing rules to EOS. A standard approach, which is commonly used in conjunction with the Peng-Robinson EOS, is the quadratic Van der Waals one-fluid mixing rule[67]. Following this rule, the two substance-specific parameters are replaced by

$$a_m = \sum_i \sum_j x_i x_j a_{ij}, \tag{10}$$

and

$$b_m = \sum_i x_i b_i, \tag{11}$$

wherein

$$a_{ij} = (1 - k_{ij})(a_i a_j)^{1/2}. \tag{12}$$

In this work, the Peng-Robinson EOS was not only used to determine vapor pressure and composition of the coexisting phases but also homogeneous density and residual enthalpy of vaporization data. For details on these calculations in the context of cubic EOS, the reader is referred to the standard literature[69]. In analogy to the approach described for the PC-SAFT EOS, it was attempted to calculate fugacity coefficients in order to obtain the Henry's law constant. Unfortunately, it was not possible to achieve even qualitative agreement with the experimental data. Therefore, solubility of the aqueous systems was not described with the Peng-Robinson EOS in the main body of this study. However, some solubility results from the Peng-Robinson EOS are shown in the supporting information.

2.5 Multiparameter Helmholtz energy equations of state

It is widely known that empirical multiparameter EOS, which are most often explicit in terms of the Helmholtz energy, are among the most accurate models for thermodynamic properties, if the underlying experimental data base is of high quality and sufficiently large. These requirements are met for several pure substances, like H_2O[70] or CO_2[71], where the uncertainty of the resulting empirical EOS is comparable to the error of the underlying experiments. Unfortunately, very few pure substances were measured that thoroughly. When considering mixtures, the necessary size of an experimental data base is even larger, since the mixture composition appears as an additional independent variable.

To date, only few empirical Helmholtz energy EOS are available for mixtures, among the most popular ones are the GERG-2008 EOS[21] and the EOS-CG[22]. Both of these EOS were adjusted to experimental binary mixture data and are able to predict the mixture behavior of higher order mixtures assuming pairwise additivity. The GERG-2008 EOS was mainly developed for the thermodynamic properties of natural gases[21] and covers 21 components, including the five present ones. Although the EOS-CG covers only six components, i.e. CO_2, H_2O, N_2, O_2, Ar and CO, it is also highly relevant here because it aims at humid combustion gases and humid or compressed air[22]. Consequently, the EOS-CG serves in this work as a reference for binary mixtures without H_2, whereas the GERG-2008 EOS was seen as a reference for systems containing H_2.

3 Results and discussion

The VLE behavior of all employed models was evaluated on the basis of vapor pressure, saturated densities and residual enthalpy of vaporization

$$\Delta h_{\mathrm{vap}}^{\mathrm{res}} = h_{\mathrm{liq}}^{\mathrm{res}} - h_{\mathrm{gas}}^{\mathrm{res}} = (h_{\mathrm{liq}} - h_{\mathrm{liq}}^{\mathrm{ideal}}) - (h_{\mathrm{gas}} - h_{\mathrm{gas}}^{\mathrm{ideal}}). \tag{13}$$

Additionally, homogeneous density and Henry's law constant data are presented. Binary, ternary and quaternary mixtures are discussed under conditions where experimental data are available for assessment. Typically, three experimental isotherms from the literature were taken to study the VLE behavior of binary mixtures. Attention was paid to selecting more than one experimental data source to assess the validity of any single measurement series. Along with a large temperature range, it was also aimed at a large composition range. Experimental pvT data were selected to allow for an extrapolation of the employed models to extreme conditions. An equimolar composition was preferred for binary pvT data because this implies that unlike interactions have the strongest influence. If possible, supercritical "liquid-like" (at high density) and supercritical "gas-like" (at low density) states were taken

into account. Deviations were evaluated using the mean absolute percentage error (MAPE) to a reference value (experimental or multiparameter EOS)

$$\mathrm{MAPE} = \frac{100}{n} \sum_{i}^{n} \left| \frac{X_{\mathrm{model,i}} - X_{\mathrm{ref,i}}}{X_{\mathrm{ref,i}}} \right|, \tag{14}$$

where n is the number of data points and X is a given thermodynamic property.

In cases where binary mixture models had to be adjusted to experimental data, only a single temperature independent parameter was allowed, cf. section 2. For molecular simulation, the binary interaction parameter ξ was either adjusted to one experimental vapor pressure data point at some intermediate temperature close to equimolar composition or, in the case of the aqueous systems, to reproduce experimental Henry's law constant data at $T \approx 320$ K because numerous measurements are available around this temperature. The adjustment of k_{ij} for the Peng-Robinson and the PC-SAFT EOS was carried out with the least squares method using the available experimental vapor pressure data.

Some of the binary mixtures presented here, namely N_2 + O_2, N_2 + Ar and Ar + O_2, were already studied by our group. Therefore, the binary interaction parameter ξ for these mixtures was taken from that preceding work[11,12]. All binary parameters are listed in Table 4. Higher order mixture data were not considered for adjustment because all of the present models assume pairwise additivity. The numerical molecular simulation data and the associated statistical uncertainties can be found in the supporting information. It has to be noted that statistical uncertainties are only shown in the figures below if they exceed symbol size.

3.1 Binary vapor-liquid equilibria

The fluid phase behavior of H_2 + N_2 is shown in Fig. 1 for three isotherms. For better visibility, the diagram was separated, showing mixture data from molecular simulation obtained with the present H_2 force field (top) and the literature force field[36] (center), respectively.

Table 4: Binary parameters for molecular models ξ, Peng-Robinson EOS k_{ij} and PC-SAFT EOS k_{ij}.

Mixture	ξ	Ref.	k_{ij} (PR EOS)	k_{ij} (PC-SAFT EOS)
Hydrogen A / B + Nitrogen	1.08 / 0.88		-0.0878	0.1248
Hydrogen A / B + Oxygen[1]	1 / 1		0	0
Hydrogen A / B + Argon	1.06 / 0.895		-0.1996	0.0962
Hydrogen A / B + Water	1.52 / 1.05		-1.4125	0.0500
Nitrogen + Oxygen	1.007	[11]	-0.0115	-0.0030
Nitrogen + Argon	1.008	[12]	-0.0037	-0.0065
Nitrogen + Water	1.07		-0.0501	0.1198
Oxygen + Water	1.00		-	-
Argon + Oxygen	0.988	[12]	0.0139	0.0086
Argon + Water	1.05		-	-

[1] Data for this binary mixture were predicted without assessment and are thus presented in the supporting information only.

Additionally, the relative volatility

$$\alpha = \frac{y_i/x_i}{y_j/x_j}, \tag{15}$$

is depicted (bottom). Sufficient experimental data are available to validate the performance of the models. This mixture shows a two-phase region that is typical if one of the components is supercritical. Among the EOS correlations, the Peng-Robinson EOS exhibits the best agreement with the experimental data, both in the saturated liquid and vapor, which also leads to a good agreement for the relative volatility. The PC-SAFT EOS overestimates the critical point and also shows an inadequate slope for the saturated liquid line at 83.15 K. None of the two empirical multiparameter EOS are shown in Fig. 1 because (a) H_2 is not implemented in the EOS-CG and (b) the GERG-2008 EOS yields a false liquid-liquid equilibrium phase separation at 83.15 K and strongly overestimates the pressure for $T >$ 83.15 K. However, cryogenic H_2 mixtures were not the main focus during the development of the GERG-2008 EOS and its normal range of validity in temperature is specified as 90 to 450 K[21], which means that the lowest isotherm is an extrapolation. More details on the performance of GERG-2008 EOS in case of H_2 mixtures are shown in the supporting information. Comparing the two H_2 force fields, the present one shows a better agreement,

cf. Fig. 1 (bottom). Especially at $T = 83.15$ K on the saturated liquid line, the use of the force field of Marx and Nielaba[36] leads to an underestimation of the vapor pressure by about 9% when compared to the Peng-Robinson EOS.

Fig. 2 shows saturated densities (top) and residual enthalpy of vaporization (bottom) for H_2 + N_2 for the same isotherms. Typically, there are no experimental mixture data available for these properties. For the reasons discussed above, no empirical multiparameter EOS results are shown. Cubic EOS, especially in their simple forms, often tend to yield a poor representation of the saturated liquid density[63], which can also be observed for this system. The saturated liquid density at 83.15 K of pure N_2 was overestimated by about 3.5 mol/l, which corresponds to a deviation of 13 % when compared to the other models and the reference EOS for pure N_2[76]. For both properties, the two H_2 force fields lead to quite similar results.

VLE properties of H_2 + Ar are depicted in Fig. 3. The separation of these diagrams into sub-diagrams was done in analogy to H_2 + N_2. When compared to H_2 + N_2, this system shows a similar shape of the phase envelope, but the vapor pressure is higher by about a factor of two at the same temperature and H_2 mole fraction. The solubility of H_2 in liquid Ar is thus lower than in liquid N_2. The agreement between the Peng-Robinson EOS, the molecular simulation data on the basis of the present H_2 force field and the experimental data is very satisfactory for the saturated liquid line. On the saturated vapor line, especially for lower temperatures, deviations of all employed models to the experimental data can be observed. This finding is validated by the relative volatility representation, cf. Fig. 3 (bottom). The PC-SAFT EOS is again characterized by an inadequate slope of the saturated liquid line and yields a critical line which is higher than expected. At lower temperatures, the molecular simulations with the literature force field for H_2, cf. Fig. 3 (center), show a similar behavior. For the same reasons as discussed before, the GERG-2008 EOS is not shown here. Saturated densities and residual enthalpy of vaporization data for H_2 + Ar are not discussed in detail because they are quite similar to H_2 + N_2. The reader is referred to

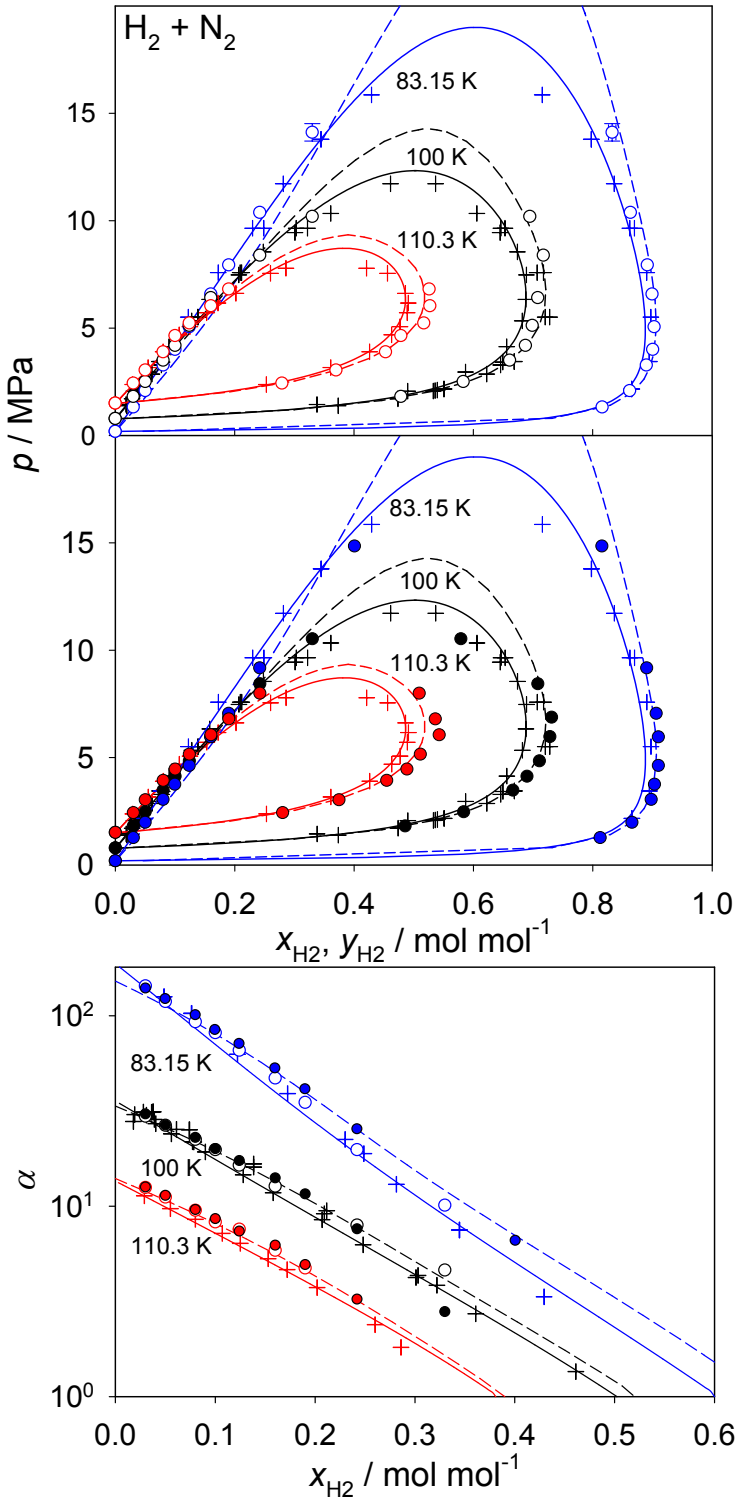

Figure 1: Isothermal fluid phase diagrams (top and center) and relative volatility (bottom) of the binary mixture H_2 + N_2: (○) Molecular simulation results obtained with the present H_2 force field or (●) with the H_2 force field of Marx and Nielaba[36], (—) Peng-Robinson EOS, (- -) PC-SAFT EOS and (+) experimental literature data[72–75]. Statistical uncertainties of the molecular simulation data are only shown if they exceed symbol size.

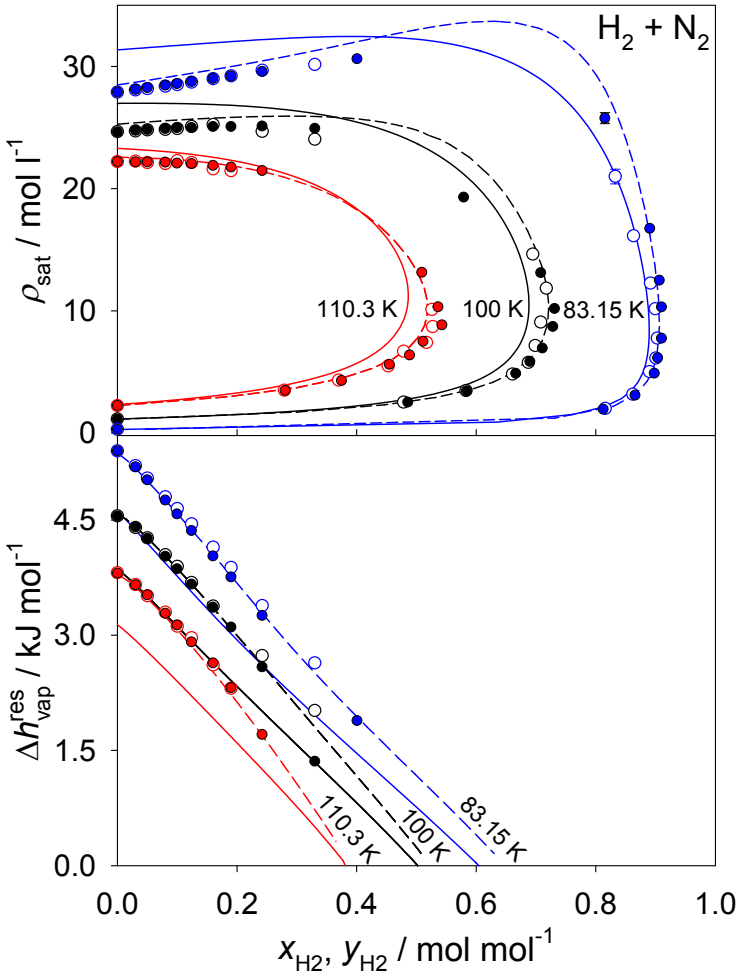

Figure 2: Isothermal saturated densities ρ_{sat} (top) and residual enthalpy of vaporization $h_{\mathrm{vap}}^{\mathrm{res}}$ (bottom) of the binary mixture H_2 + N_2: (○) Molecular simulation results obtained with the present H_2 force field or (●) with the H_2 force field of Marx and Nielaba[36], (—) Peng-Robinson EOS and (- -) PC-SAFT EOS. Statistical uncertainties of the molecular simulation data are only shown if they exceed symbol size.

the supporting information for more information.

The vapor pressure of H_2 + H_2O is shown in Fig. 4 for two isotherms. This system is characterized by a low solubility of H_2 in liquid H_2O. It has to be noted that a scale break on the horizontal axis had to be applied to make the results for the saturated liquid line of this mixture discernible. Experimental data to assess the quality of the present models are scarce and relatively old. The agreement of the molecular simulation results from both force fields with the experimental data is satisfactory on the saturated liquid line, whereas deviations are larger for the saturated vapor. As opposed to this, all employed EOS perform well on the saturated vapor line. As before, the GERG-2008 EOS predicts a liquid-liquid equilibrium for this mixture. The saturated liquid line from the PC-SAFT EOS is similar to the results obtained by molecular simulation. No relative volatility data are presented here for the VLE of aqueous systems because no composition data for the saturated liquid and vapor were available at the same vapor pressure.

N_2 and O_2 are the main components of air, therefore the VLE properties of this mixture are of central importance, e.g. for air liquefaction. A molecular simulation study on this system was conducted by Stoll et al.[11], using the same pure component force fields. Their results agree extraordinarily well with experimental vapor pressure data from the literature, cf. Fig. 5 (top). Fig. 5 (bottom) allows for a more precise examination of this binary mixture. It can be seen that the molecular simulation data exhibit larger deviations at $T = 80$ K for both small concentrations of N_2 and small concentrations of O_2. Around equimolar composition, the agreement is better. It has to be noted that this system is rather simple (both components are similiar, subcritical and the mixture is zeotropic) such that all other employed modeling approaches perform very well.

The saturated densities and the residual enthalpy of vaporization of N_2 + O_2 are shown in Fig. 6. It has to be noted that there is a scale break on the vertical axis of the top diagram, dividing it into saturated liquid density (above the break) and saturated vapor density (below the break). For this system, the EOS-CG can be used as a reference. It is striking that the

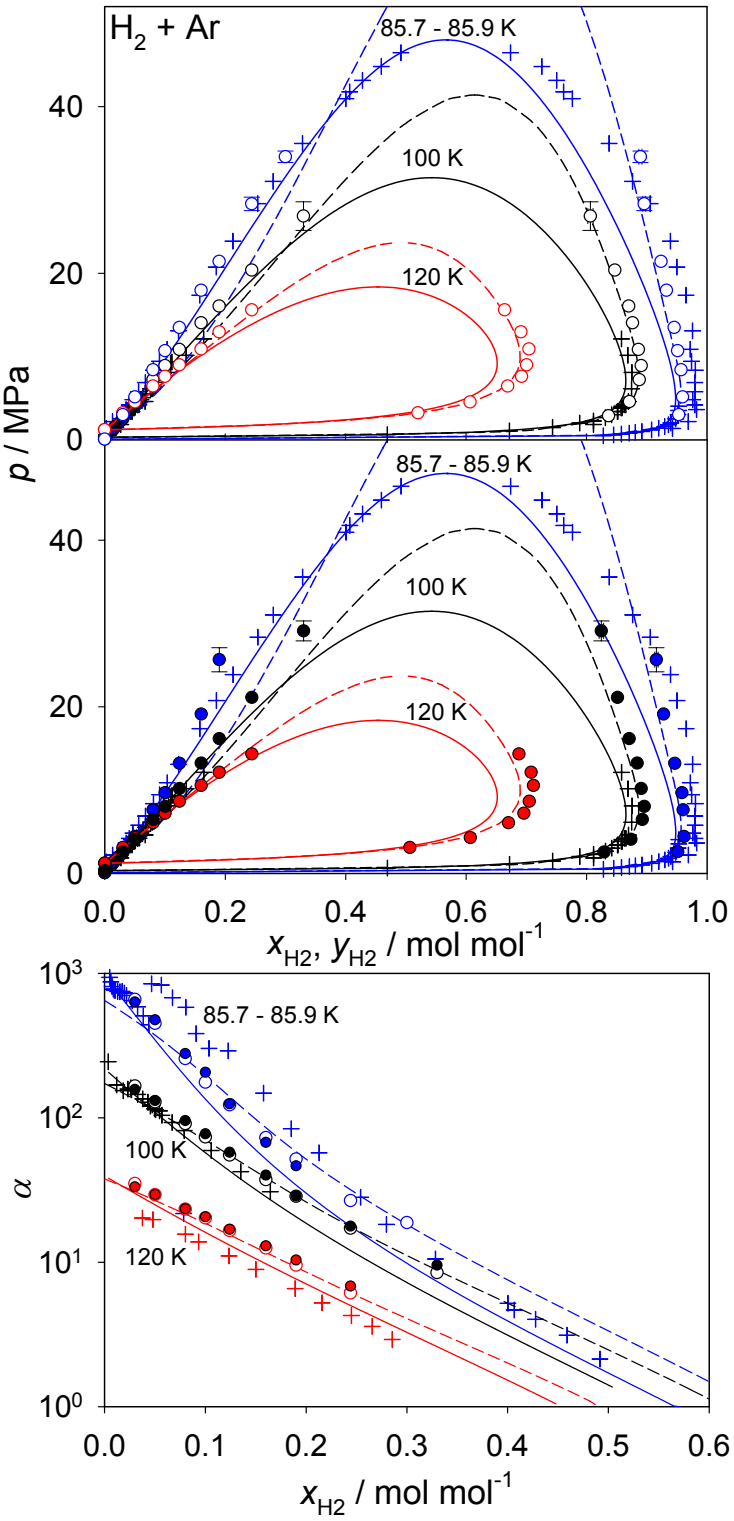

Figure 3: Isothermal fluid phase diagrams (top and center) and relative volatility (bottom) of the binary mixture H_2 + Ar: (○) Molecular simulation results obtained with the present H_2 force field or (●) with the H_2 force field of Marx and Nielaba[36], (—) Peng-Robinson EOS, (- -) PC-SAFT EOS and (+) experimental literature data[75,77–80]. Statistical uncertainties of the molecular simulation data are only shown if they exceed symbol size.

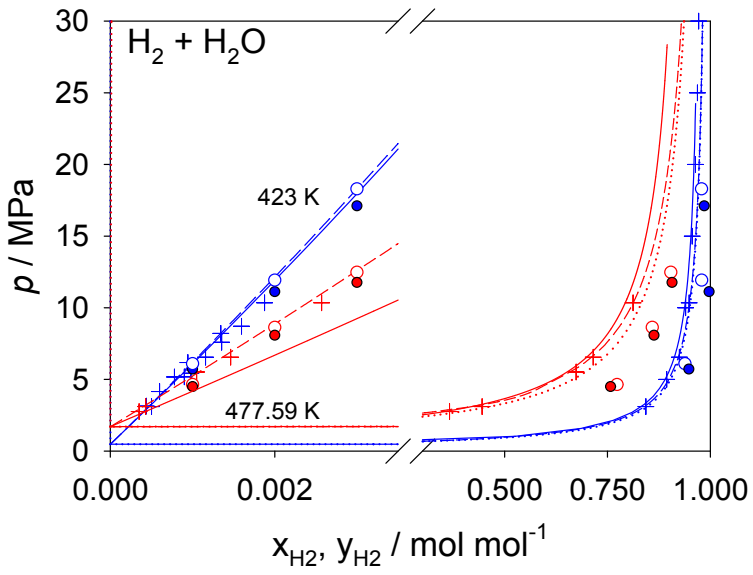

Figure 4: Isothermal fluid phase diagram of the binary mixture H_2 + H_2O: (○) Molecular simulation results obtained with the present H_2 force field or (●) with the H_2 force field of Marx and Nielaba[36], (—) Peng-Robinson EOS, (- -) PC-SAFT EOS, (· · ·) GERG-2008 EOS and (+) experimental literature data[81–85].

saturated liquid density from molecular simulation agrees exceptionally well with the EOS-CG, exhibiting a MAPE value of 0.2 %. The PC-SAFT EOS performs also quite well, i.e. the MAPE is 1.0 %, and is even preferable to the molecular simulation data for the saturated vapor at $T = 120$ K (0.4 % versus 2.4 % MAPE). Again, the Peng-Robinson EOS leads to an overestimation of the saturated liquid density, which becomes increasingly severe with increasing density. The residual enthalpy of vaporization was reproduced satisfactorily by all present models. At $T = 120$ K and larger mole fractions of N_2, the PC-SAFT EOS is superior to both molecular simulation and the Peng-Robinson EOS.

N_2 + H_2O is presented in a similar manner as H_2 + H_2O, cf Fig. 7. Two isotherms were used to asses the quality of the present models. There is, however, a discrepancy between the different experimental data sources on the saturated liquid line for both isotherms. Therefore, a precise evaluation is difficult. Nonetheless, both molecular simulation and the PC-SAFT EOS show reliable results for the saturated liquid, whereas EOS-CG and the Peng-Robinson EOS deviate, especially at $T = 573.15$ K. The agreement of molecular simulation with

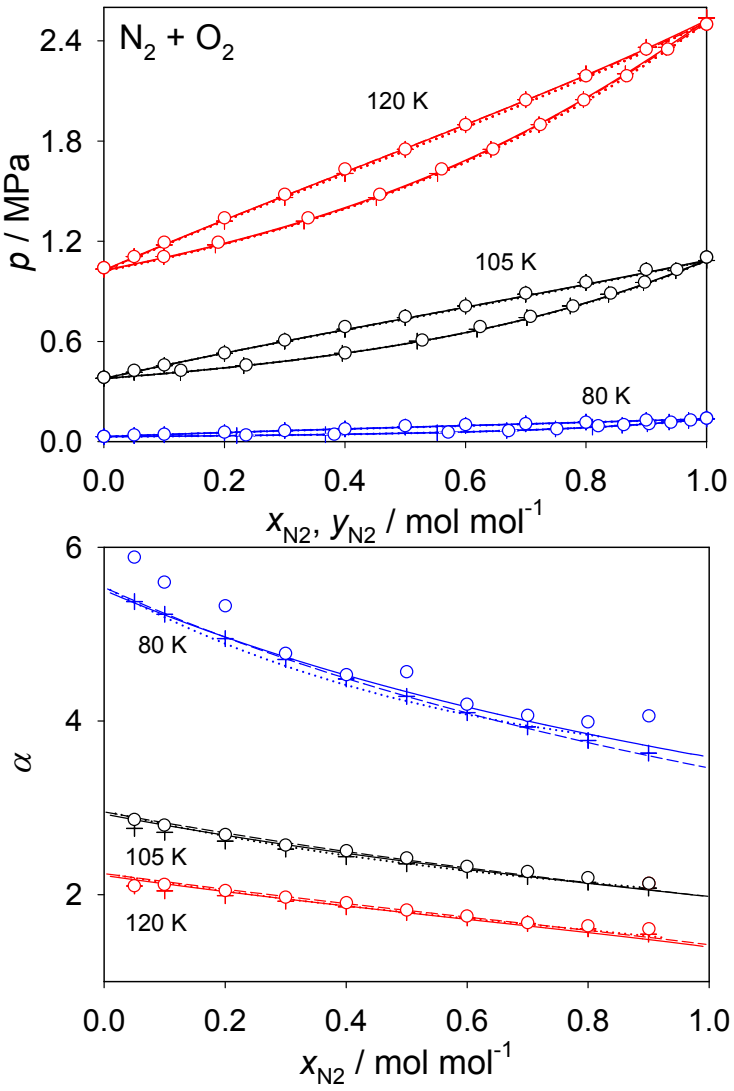

Figure 5: Isothermal fluid phase diagram (top) and relative volatility (bottom) of the binary mixture $N_2 + O_2$: (○) Molecular simulation results, (—) Peng-Robinson EOS, (- -) PC-SAFT EOS, (· · ·) EOS-CG and (+) experimental literature data[86,87].

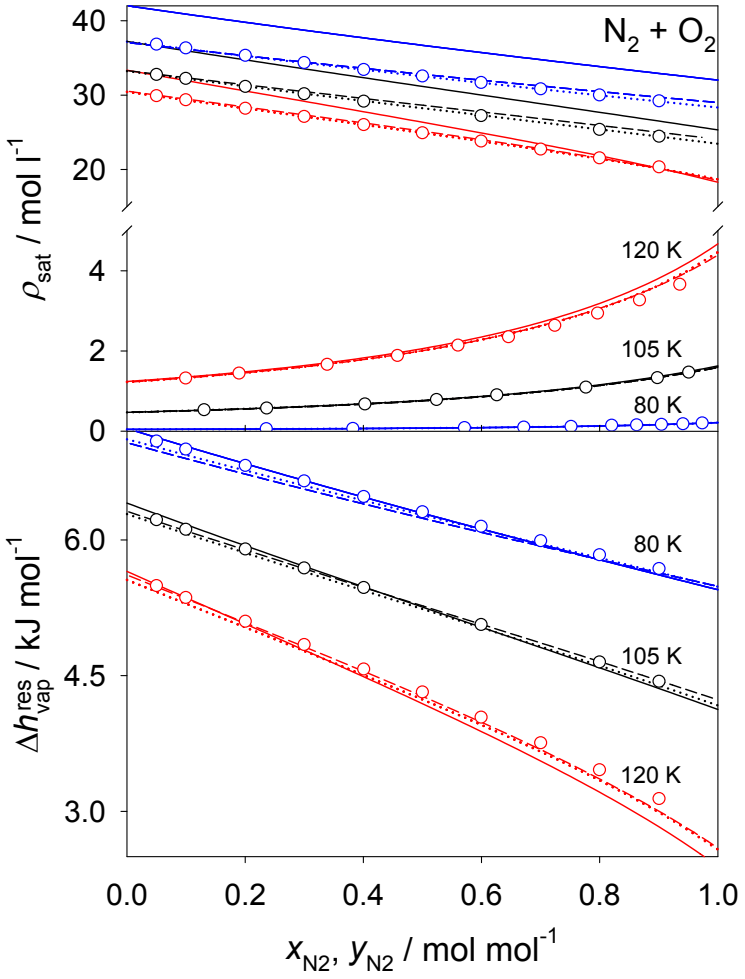

Figure 6: Isothermal saturated densities ρ_{sat} (top) and residual enthalpy of vaporization $h_{\mathrm{vap}}^{\mathrm{res}}$ (bottom) of the binary mixture N_2 + O_2: (○) Molecular simulation results, (—) Peng-Robinson EOS, (- -) PC-SAFT EOS and (· · ·) EOS-CG.

experimental data on the saturated vapor line is good. All employed EOS perform better at $T = 473.15$ K than at $T = 573.15$ K on the saturated vapor line.

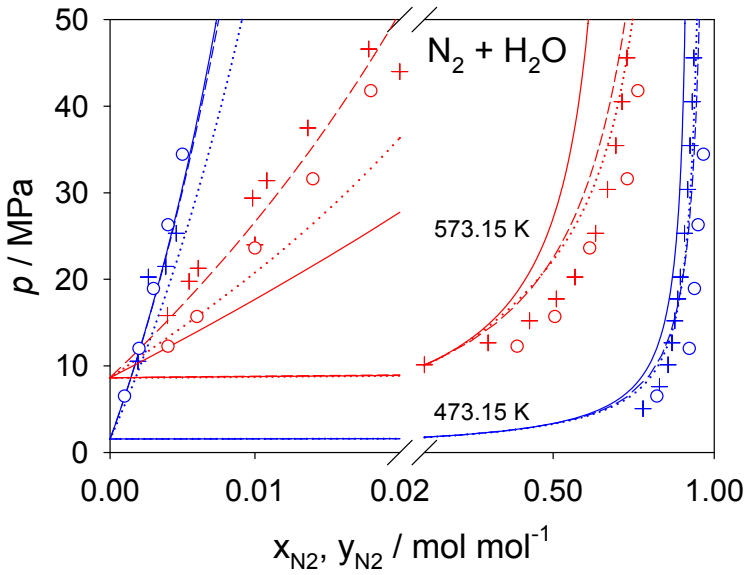

Figure 7: Isothermal fluid phase diagram of the binary mixture N_2 + H_2O: (○) Molecular simulation results, (—) Peng-Robinson EOS, (- -) PC-SAFT EOS, (· · ·) EOS-CG and (+) experimental literature data[88–91].

The remaining two binary mixtures for which classical VLE properties were investigated are N_2 + Ar and Ar + O_2. Both of these systems were in the focus of our group before so that the binary interaction parameter ξ was already adjusted to experimental data in Ref.[12] and was simply adopted here. The performance of these molecular models was evaluated in a work of Vrabec et al.[28] for the vapor pressure along a single isotherm. Therefore, the present work complements this study by providing results for a larger temperature range and additional mixture properties.

The vapor pressure of N_2 + Ar is depicted in Fig. 8 (top), showing a similar mixture behavior to that of N_2 + O_2. The agreement of molecular simulation, the PC-SAFT and the Peng-Robinson EOS in comparison to EOS-CG is excellent for the vapor pressure, i.e. MAPE values of 0.8 %, 0.6 % and 0.4 % were achieved. A more precise evaluation of the performance of all models is possible by looking at the relative volatility, cf. Fig. 8 (bottom).

In this magnified view, it can be seen that the experimental uncertainties are significant. All models lie within that scatter. Saturated densities and residual enthalpy of vaporization of this system are depicted in the supporting information.

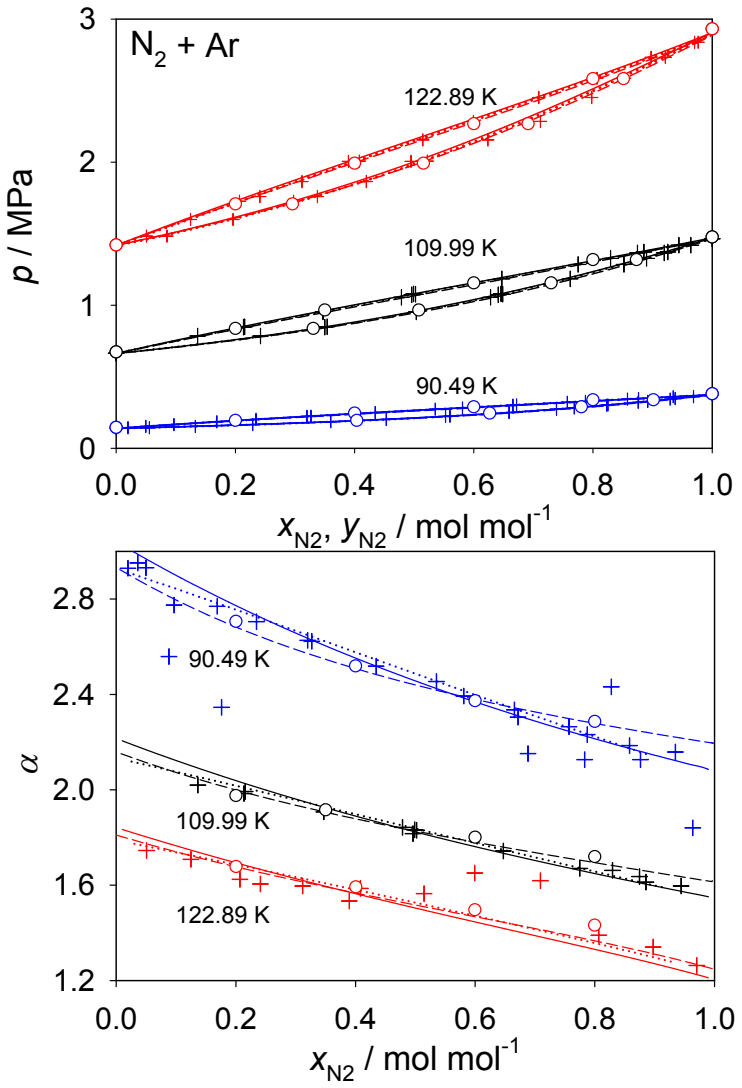

Figure 8: Isothermal fluid phase diagram (top) and relative volatility (bottom) of the binary mixture N_2 + Ar: (○) Molecular simulation results, (—) Peng-Robinson EOS, (- -) PC-SAFT EOS, (· · ·) EOS-CG and (+) experimental literature data[92,93].

Ar and O_2 are substances with very similar macroscopic properties, e.g. their critical point, that differs only by 4 K in temperature and 0.2 MPa in pressure. Mixing these substances leads to a very narrow two-phase region and an essentially ideal mixing behavior, which was reproduced almost perfectly by all present models, cf. Fig. 9 (top). When

compared to the EOS-CG, MAPE values of 0.2 % for the Peng-Robinson EOS, 0.2 % for the PC-SAFT EOS and 0.9 % for molecular simulation data were achieved for the vapor pressure. All considered EOS show a similar behavior with respect to the relative volatility, cf. Fig. 9 (bottom), and deviate from experimental data only at the lowest isotherm, whereas molecular simulation data show some deviation. Due to the similarity of the two components, the saturated mixture densities are almost constant over the whole composition range, cf. Fig. 10 (top). Both molecular based models, i.e. atomistic simulations and the PC-SAFT EOS, predict this behavior equally well, whereas the Peng-Robinson EOS deviates by a constant offset of 5 mol/l in terms of the saturated liquid density. Some discrepancies between all models were observed for the residual enthalpy of vaporization, which is shown in Fig. 10 (bottom). For this property, the EOS-CG shows a somewhat more convex shape than molecular simulation, the PC-SAFT and the Peng-Robinson EOS.

Binary VLE data for the mixtures H_2 + O_2, O_2 + H_2O and Ar + H_2O are not presented due to the lack of sufficient high quality experimental data. The aqueous systems were, however, investigated on the basis of Henry's law constant.

3.2 Binary homogeneous pvT data

Beyond VLE properties, there is also interest in homogeneous pvT data, which are discussed for binary mixtures in this section. An equimolar composition was chosen because a maximal occurence of unlike molecular interactions was targeted. Fig. 11 presents the homogeneous density for H_2 + N_2 (top) and the compressibility factor Z for H_2 + Ar (bottom), both properties were evaluated at given pressure and composition along isotherms. Z was chosen for the latter mixture, because the considered experimental data are dominated by ideal gas behavior. Unfortunately, no experimental data at higher densities were available in the vicinity of equimolar composition. In contrast to the saturated densities of the systems containing H_2 as discussed e.g. in Fig. 2, the GERG-2008 EOS is applicable under these conditions. Therefore, a better assessment of the models with respect to the density is

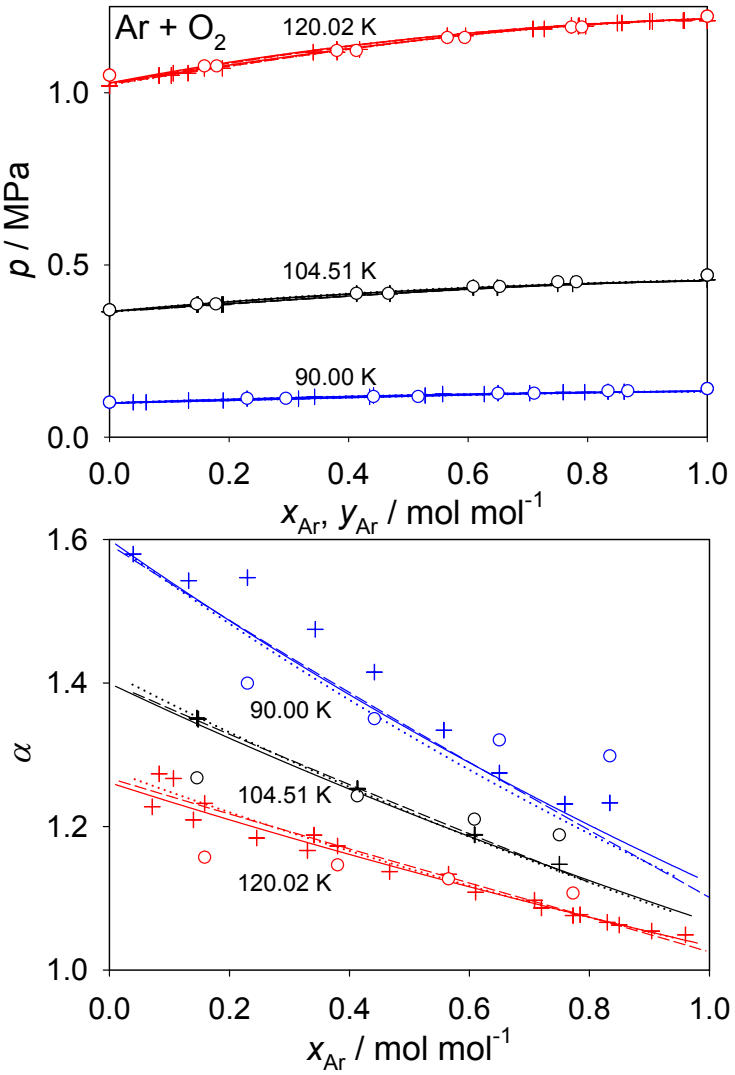

Figure 9: Isothermal fluid phase diagram (top) and relative volatility (bottom) of the binary mixture Ar + O_2: (○) Molecular simulation results, (—) Peng-Robinson EOS, (- -) PC-SAFT EOS, (· · ·) EOS-CG and (+) experimental literature data[94–96].

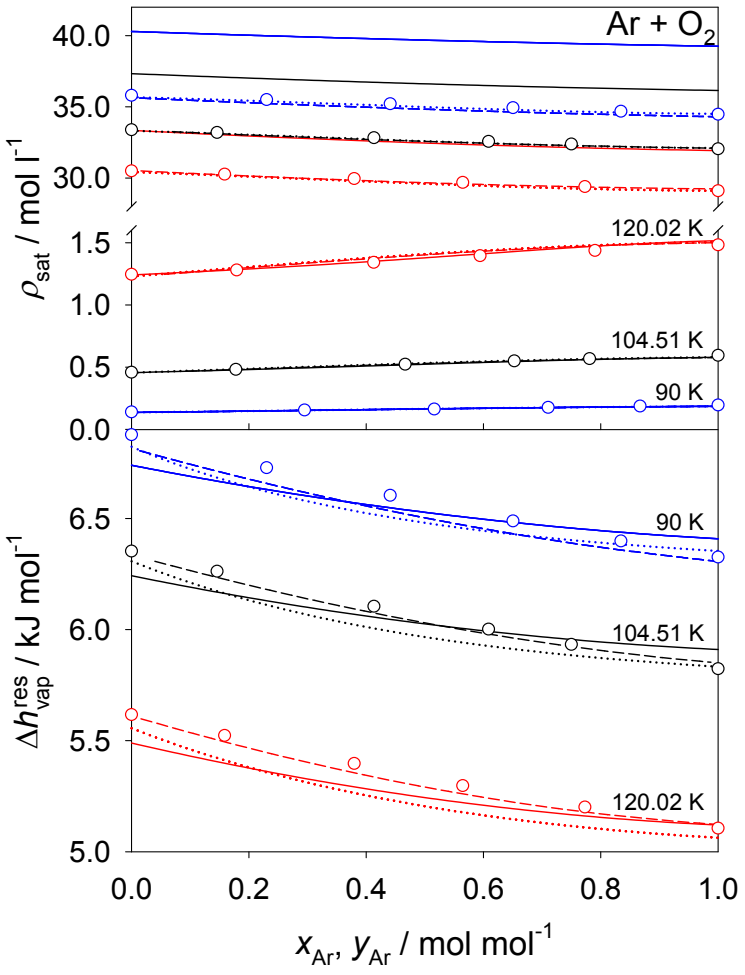

Figure 10: Isothermal saturated densities ρ_{sat} (top) and residual enthalpy of vaporization $h_{\mathrm{vap}}^{\mathrm{res}}$ (bottom) of the binary mixture Ar + O_2: (○) Molecular simulation results, (—) Peng-Robinson EOS, (- -) PC-SAFT EOS and (· · ·) EOS-CG.

feasible.

For H_2 + N_2, a large pressure and density range was covered by experimental studies, cf. Fig. 11 (top). Both the horizontal and the vertical axes have a scale break, showing a supercritical "gas-like" isotherm at $T = 273.15$ K and supercritical "liquid-like" isotherms at $T = 323.13$ K and 373.12 K. All models perform very well at $T = 273.15$ K and exhibit MAPE of ≤ 1 %. For elevated pressure and density, however, the discrepancies become larger. This applies in particular to all EOS, which tend to overestimate the density. The atomistic molecular simulations, both with the present (MAPE 0.7 %) and the H_2 force field from the literature[36] (MAPE 0.9 %) perform very well.

The experimental data base for the mixture H_2 + Ar is smaller, measurements are available up to pressures of 9 MPa, cf. Fig. 11 (bottom). Over the whole pressure range, the atomistic molecular simulations, the PC-SAFT and the GERG-2008 EOS perform well, whereas the Peng-Robinson EOS deviates qualitatively. Accordingly, MAPE of 0.3 %, 1.0 %, 0.5 %, 0.4 % and 0.7 % were found for the PC-SAFT EOS, the Peng-Robinson EOS, molecular simulation with the present force field, molecular simulation with the literature force field and the GERG-2008 EOS at $T = 231.7$ K, respectively.

The homogeneous pvT behavior of three binary mixtures without H_2, i.e. N_2 + O_2, N_2 + Ar and Ar + O_2, is illustrated in Fig. 12. Experimental data and the EOS-CG were used to assess the quality of the molecular simulation data, the PC-SAFT and the Peng-Robinson EOS.

For the system N_2 + O_2, cf. Fig. 12 (top), two isotherms at intermediate pressures are presented. At 293.15 K and low density, hardly any difference between the employed models and the experimental data can be observed. Peng-Robinson EOS, PC-SAFT EOS, EOS-CG and molecular simulation have MAPE of 1.1 %, 0.5 %, 0.1 % and 0.3 %, respectively. The isotherm at $T = 142.25$ K is below the critical temperature of O_2 ($T_{c,O2} = 154.6$ K), therefore, a VLE of the mixture is conceivable. Consequently, the EOS-CG predicts the critical point of N_2 + O_2 at $p = 4.44$ MPa and $x_{N2} = 0.454$ mol·mol^{-1} at this temperature.

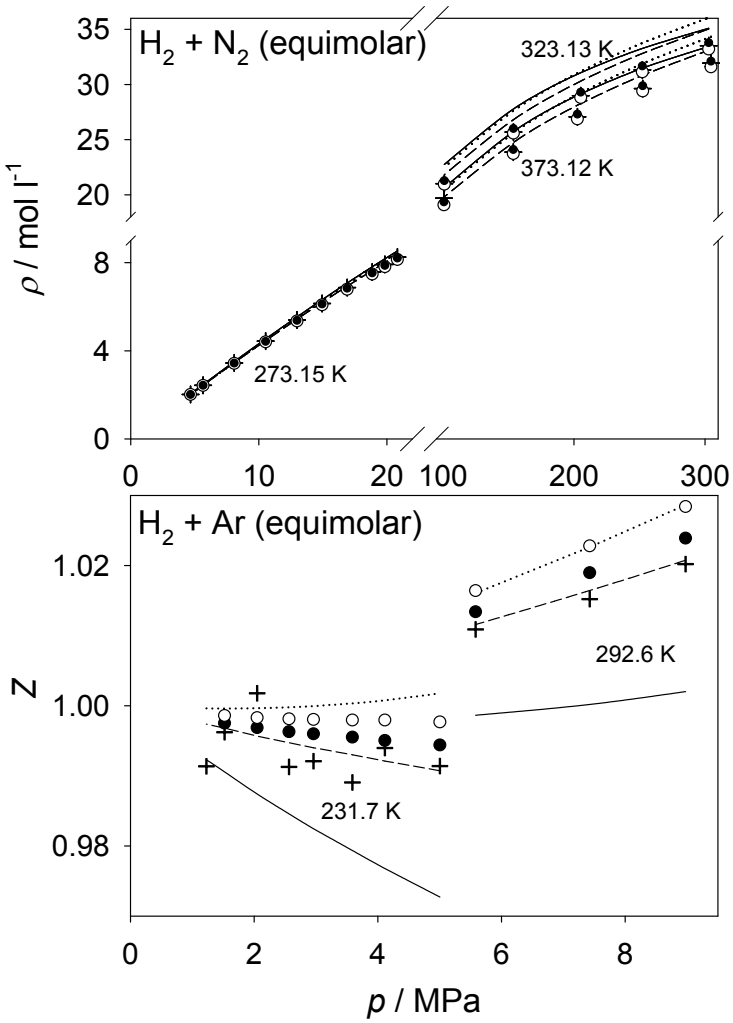

Figure 11: Homogeneous density ρ of the binary mixture H_2 + N_2 (top) and the compressibility factor Z of the binary mixture H_2 + Ar (bottom) at equimolar composition along isotherms: (○) Molecular simulation results obtained with the present H_2 force field or (●) with the H_2 force field of Marx and Nielaba[36], (—) Peng-Robinson EOS, (- -) PC-SAFT EOS, (· · ·) GERG-2008 EOS and (+) experimental literature data[97–99].

The shape of this isotherm can therefore be explained by a close passing of the critical line of this mixture, starting from a "gas-like" state and ending in a "liquid-like" state. It can be seen that the EOS-CG shows the best agreement with the experimental data. Close to the mixtures' critical line, molecular simulation data show the largest deviations, which may be caused by finite size effects. State points that are not in the vicinity of the critical line agree satisfactorily with the experimental data. The PC-SAFT and Peng-Robinson EOS agree well with each other, but fail to reproduce the reference data in the "liquid-like" region.

Fig. 12 (center) shows three isotherms for N_2 + Ar. The results are comparable and indicate a tendency that has been observed before. Namely, a good agreement to the reference data at low density was achieved by all employed models, whereas deviations become increasingly severe for the Peng-Robinson EOS and, to a limited extent, also for the PC-SAFT EOS at higher density. Results from molecular simulation agree excellently with both the experimental data and the EOS-CG, exhibiting a MAPE value of 0.4 %. For Ar + O_2 only one isotherm at low densities could be examined, which was done here in terms of the compressibility factor, cf. Fig. 12 (bottom). The best agreement to both experimental data and the EOS-CG was found for the molecular simulation data, whereas the Peng-Robinson and PC-SAFT EOS deviate more or less thoroughly.

3.3 Henry's law constant

Henry's law constant data were used in the present work to assess aqueous systems, i.e. H_2, N_2, O_2 or Ar in H_2O. This property is typically employed in cases where a solute is only little soluble in a solvent. Various definitions of the Henry's law constant are established in the literature. The present work considers the purely temperature dependent Henry's law constant, which requires that the solvent is in its saturated liquid state. Consequently, Henry's law constant data are presented from the triple point temperature to the critical temperature of H_2O. In order to validate the results of the present work, both experimental data and the official IAPWS correlation[104,105] of these data were used.

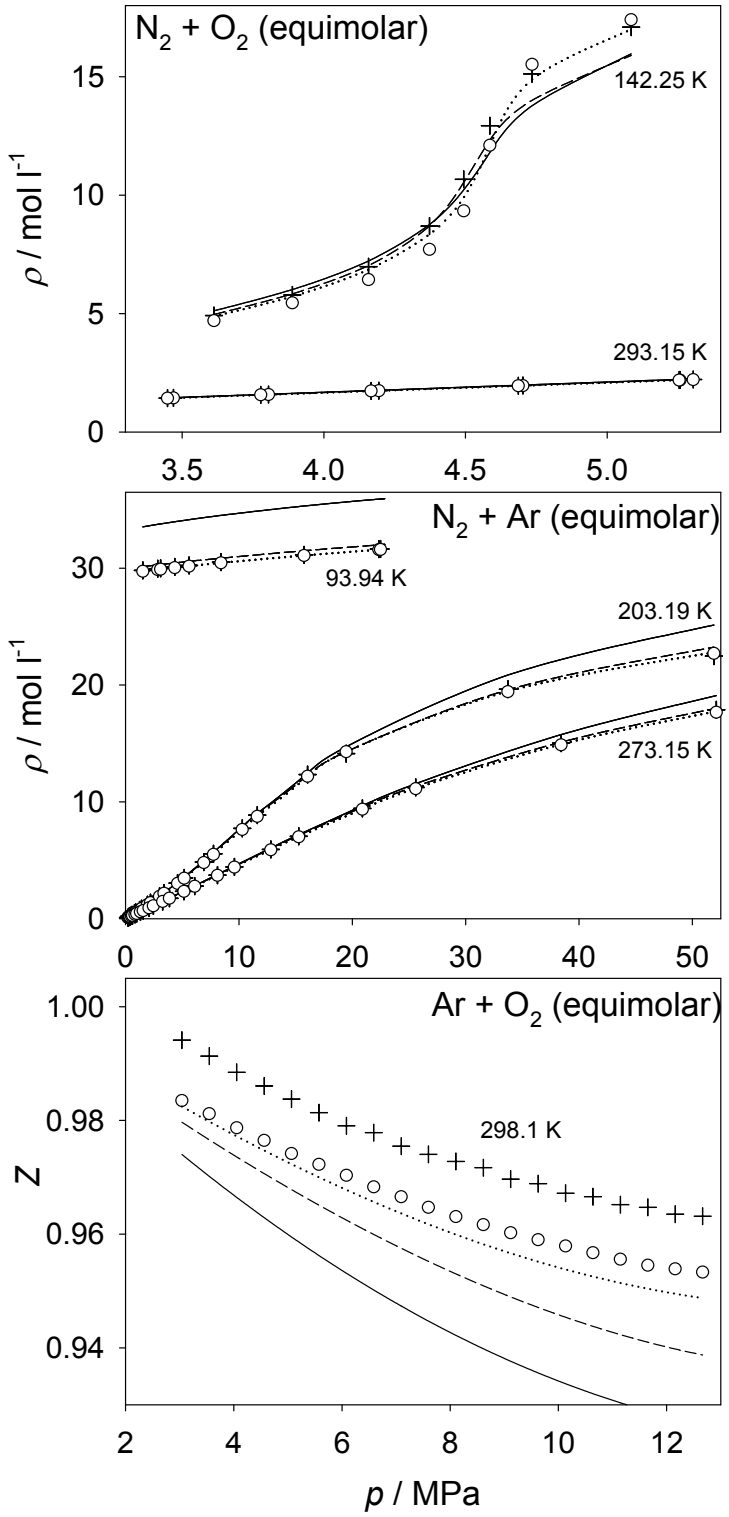

Figure 12: Homogeneous density ρ of the binary mixtures N_2 + O_2 (top), N_2 + Ar (center) and the compressibility factor Z of the binary mixture Ar+O_2 (bottom) at equimolar composition along isotherms: (∘) Molecular simulation results, (—) Peng-Robinson EOS, (- -) PC-SAFT EOS, ($\cdots$) EOS-CG and (+) experimental literature data[100–103].

All considered aqueous systems exhibit a qualitatively similar, strongly non-monotonic behavior, cf. Fig. 13. A pronounced maximum of the Henry's law constant is passed between 330 and 370 K. Note that large values of the Henry's law constant correspond to a low solubility, therefore, the solubility decreases with increasing temperature, passes through a minimum and then increases again. However, quantitative differences between the solutes are present. Close to the triple point temperature, H_2 and N_2 are almost equally soluble in H_2O ($H_{H2} \approx H_{N2} \approx 6$ GPa), but roughly three times less soluble than O_2 and Ar ($H_{O2} \approx H_{Ar} \approx 2$ GPa). Furthermore, the maximum values of the Henry's law constant differ significantly.

The results from molecular simulation are satisfactory, the region of increasing Henry's law constant at low temperature was reproduced almost perfectly for all four solutes, whereas deviations are present at intermediate temperatures for N_2, O_2 and Ar. For H_2, the agreement to the reference data is satisfying throughout for both employed force fields. Nonetheless, a disadvantage of the present force field for H_2 becomes apparent here. In order to compensate the missing electrostatic interactions of H_2, which are obviously very important when H_2O is involved, the unlike LJ interaction energy had to be increased. This fact is reflected by a rather unphysically large value of $\xi = 1.52$.

The EOS-CG fails to reproduce the solubility data for Ar even qualitatively and predicts a monotonically decreasing Henry's law constant for increasing temperature. For N_2 and O_2, that behavior is predicted in a qualitatively correct way, but deviates quantitatively from the IAPWS reference. An application of the Henry's law constant to the fitting algorithms for empirical Helmholtz energy EOS should therefore be considered in the future.

3.4 Ternary vapor-liquid equilibria

For higher order mixtures smaller experimental data bases can be found in the literature. Consequently, only for two of the ten possible ternary systems experimental VLE data are available for comparison, i.e. N_2 + O_2 + Ar and H_2 + N_2 + Ar. Since all models ap-

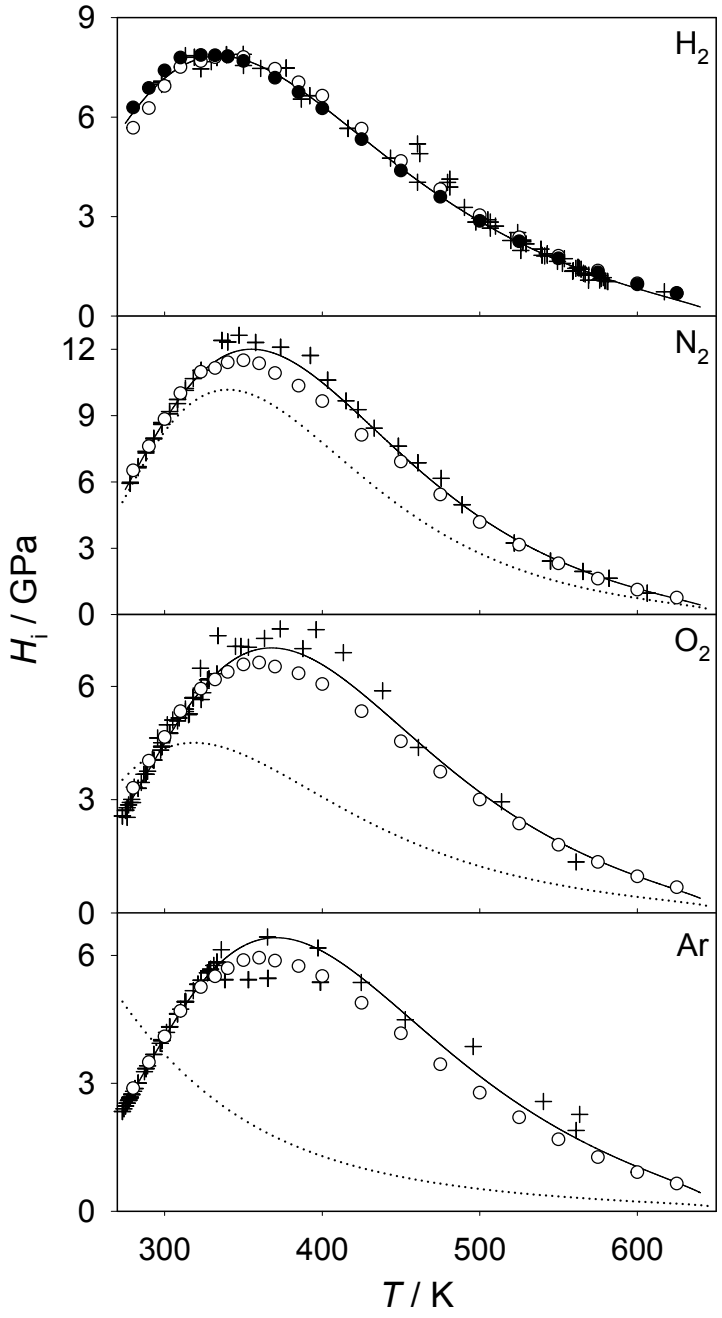

Figure 13: Henry's law constant of H_2, N_2, O_2 and Ar in H_2O (from top to bottom): (○,●) Molecular simulation results (H_2: (○) Present force field, (●) force field of Marx and Nielaba[36]), (—) official IAPWS guideline[104,105], (· · ·) EOS-CG and (+) experimental literature data (H_2[106,107]; N_2[107–110]; O_2[111–114]; Ar[115–118]).

plied in this study are based on pairwise additivity and neglect higher order interactions, the presented results are considered as predictive. This also applies to the EOS-CG and the GERG-2008 EOS, therefore, mainly experimental data were used as a reference for higher order mixtures. The following ternary VLE diagrams show the saturated mixture compositions at constant temperature and pressure.

Fig. 14 depicts the VLE for N_2 + O_2 + Ar (dry air) which was already examined in molecular simulation studies of our group[13,14]. This system is characterized by a comparably narrow two-phase region. At $T = 83.6$ K and pressures of about $p = 0.13$ MPa, cf. Fig. 14, the experimental data seem to scatter considerably, but this is rather caused by their small temperature and pressure variations. Molecular simulations were specified to reproduce the experimental data on the saturated liquid line and therefore seemingly scatter as well. Nonetheless, the agreement of all employed models is satisfactory. Especially the PC-SAFT EOS and the EOS-CG agree quite well.

A VLE phase diagram of H_2 + N_2 + Ar is presented in Fig. 15. This system exhibits a large two-phase region due to the presence of H_2. An excellent agreement between the molecular simulation data, the PC-SAFT EOS and the experimental data on the saturated liquid and vapor line was observed. The GERG-2008 EOS predicts the saturated vapor line satisfactorily, but deviates from the experiments when the saturated liquid line is considered, whereas the Peng-Robinson EOS predicts a two-phase region that is slightly too narrow. Additional ternary VLE data for both of these mixtures can be found in the supporting information.

3.5 Higher order homogeneous *pvT* data

Although any higher order mixture could be targeted with the considered modeling approaches, the present study is limited by experimental data availability. Therefore, homogeneous pvT data are only presented for one ternary and one quaternary system, i.e. N_2 + O_2 + Ar (dry air) and N_2 + O_2 + Ar + H_2O (humid air), respectively. For both mixtures,

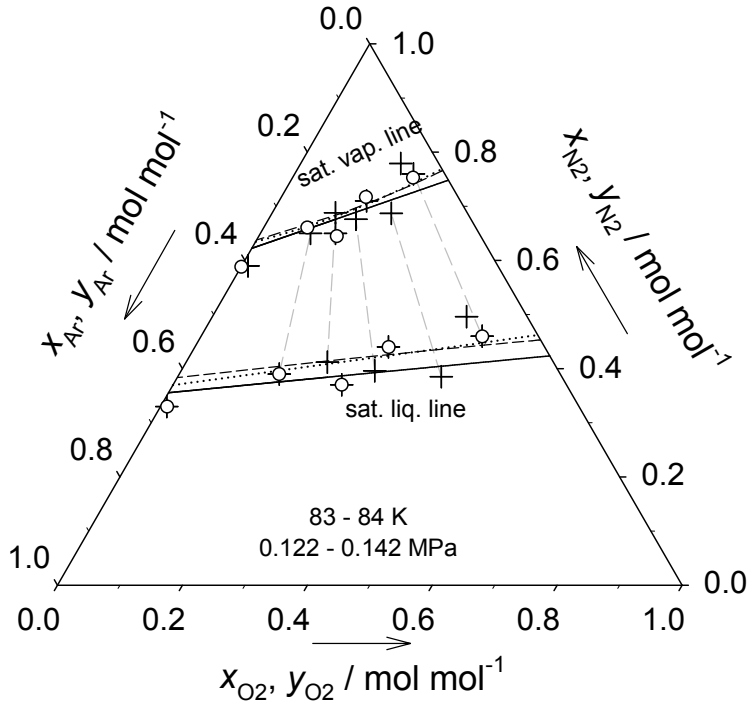

Figure 14: Fluid phase diagram of the ternary system N_2 + O_2 + Ar at 83 to 84 K and 0.122 to 0.142 MPa: (○) Molecular simulation results, (—) Peng-Robinson EOS, (- -) PC-SAFT EOS, (· · ·) EOS-CG and (+) experimental literature data[119].

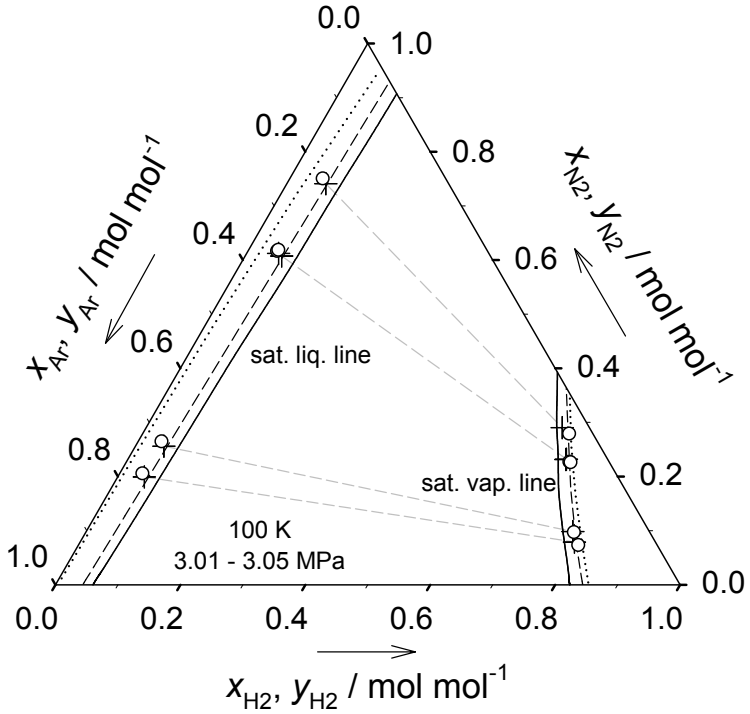

Figure 15: Fluid phase diagram of the ternary system H_2 + N_2 + Ar at 100 K and 3.01 to 3.05 MPa: (○) Molecular simulation results, (—) Peng-Robinson EOS, (- -) PC-SAFT EOS, (· · ·) GERG-2008 EOS and (+) experimental literature data[75].

large temperature and pressure ranges were studied.

The homogeneous pvT behavior along four isotherms for N_2 + O_2 + Ar is shown in Fig. 16. Experimental data are available at $T \leq 873.19$ K and $p \leq 70$ MPa. In this case, a high quality Helmholtz energy explict EOS for standard dry air by Lemmon et al.[120] was used as a reference. The experimental data were predicted well by molecular simulation, the EOS-CG and the PC-SAFT EOS with MAPE of 0.6 %, 0.2 % and 1.1 %, respectively. At $T = 70$ K, where dry air is in its liquid state, the Peng-Robinson EOS shows large deviations. It can be seen that the EOS-CG and the molecular simulation data agree well to the dry air EOS by Lemmon et al.[120] for pressures above 70 MPa in the gaseous phase, whereas the Peng-Robinson and the PC-SAFT EOS deviate more or less thoroughly. In the liquid state, molecular simulation data and the PC-SAFT EOS overestimate the density on average by 0.6 % and 1.8 % (MAPE), respectively.

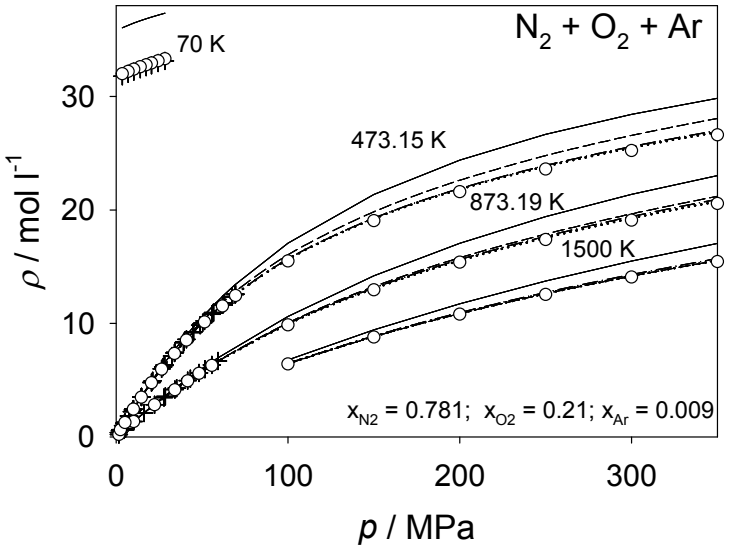

Figure 16: Homogeneous density ρ of the ternary mixture N_2 + O_2 + Ar at a composition which represents dry air along four isotherms: (○) Molecular simulation results, (—) Peng-Robinson EOS, (- -) PC-SAFT EOS, (· · ·) EOS-CG, (-·-) dry air EOS by Lemmon et al.[120] and (+) experimental literature data[121–123].

Two different compositions are discussed for the quaternary system N_2 + O_2 + Ar + H_2O, the first corresponding to humid air, cf. Fig. 17 (top), and the second corresponding

to supercritical H_2O containing a substantial amount of solved gases, cf. Fig. 17 (bottom). Since no adjustment of the PC-SAFT and the Peng-Robsinon EOS could be carried out for the subsystems O_2 + H_2O and Ar + H_2O due to the lack of experimental data, their binary interaction parameter was set to $k_{ij} = 0$ for these calculations. Although plenty of experimental measurements were conducted for humid air, only one experimental data point is shown here due to varying temperatures and compositions in the experiment series. Over the whole range of temperature and pressure, the agreement between the EOS-CG and the present molecular simulations is excellent, a MAPE of 0.8 % was found. The PC-SAFT and the Peng-Robinson EOS differ more or less strongly from the EOS-CG and yield MAPE of 1.5 % and 5.4 %, respectively. Fig. 17 (bottom) shows a "water-like" composition of the four discussed substances. It is interesting that the EOS-CG reproduces the experimental data very well at lower pressures, whereas molecular simulation is superior at higher pressures. One cause for the deviation of the molecular simulation results at lower pressures could be the close proximity to the critical point of this mixture, i.e. water as the main component has critical properties of $T_c = 647.1$ K, $p_c = 22$ MPa and $\rho_c = 17.87$ mol/l. The best agreement for this mixture was found for the PC-SAFT EOS, whereas the Peng-Robinson EOS deviates strongly from the experimental data at high pressures.

4 Conclusion

Several models were applied to describe the mixture behavior of five substances that are relevant for hydrogen technology. In a first step, available pure component force fields were complemented by a new force field for H_2 and subsequently adjusted to reproduce the fluid phase behavior of all involved binary mixtures. This was done by fitting a single temperature independent parameter to experimental vapor pressure data of binary mixtures or, in the case of the aqueous systems, to one experimental Henry's law constant data point. The primary focus was on molecular simulation, however, also a molecular based

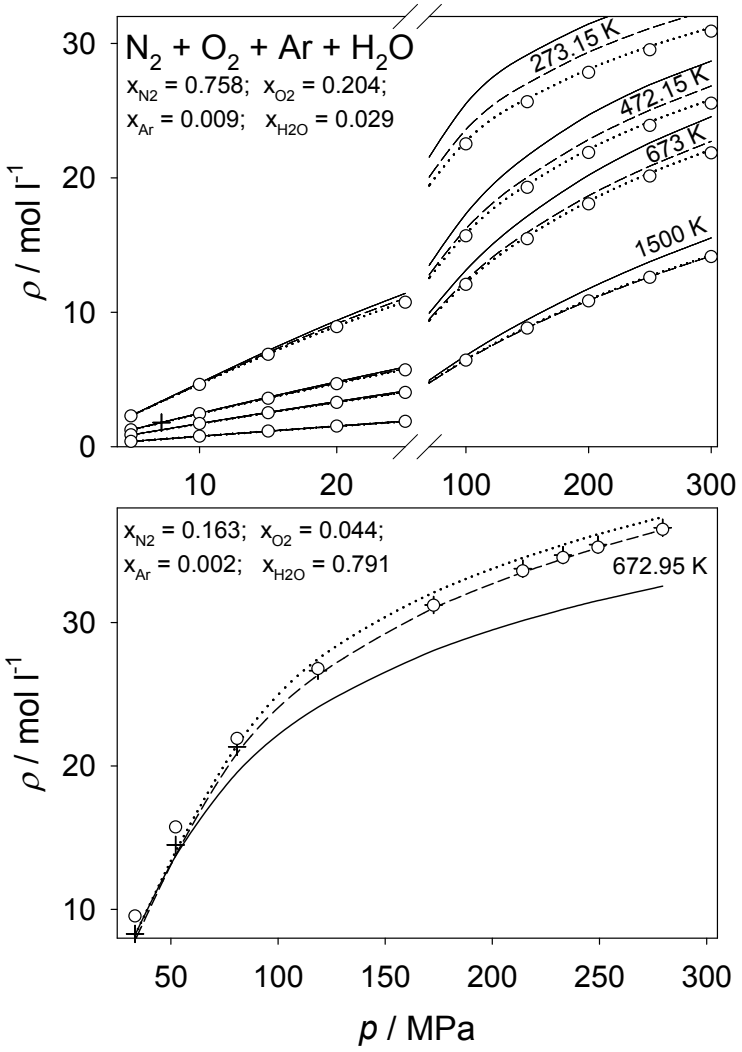

Figure 17: Homogeneous density ρ of the quaternary mixture N_2 + O_2 + Ar + H_2O along four isotherms at a composition which represents humid air (top) and supercritical H_2O containing ≈ 0.2 mol·mol^{-1} of air components (bottom): (∘) Molecular simulation results, (—) Peng-Robinson EOS, (- -) PC-SAFT EOS, (···) EOS-CG and (+) experimental literature data[124,125].

EOS (PC-SAFT EOS) and empirical EOS of different complexity (Peng-Robinson EOS, GERG-2008 EOS and EOS-CG) were studied. In addition to VLE properties, i.e. vapor pressure, saturated densities and residual enthalpy of vaporization, also the pvT behavior and solubility were considered. Furthermore, the thermodynamic properties of higher order mixtures were predicted assuming pairwise additivity throughout.

Not all of the employed models could be used for every system or thermodynamic property under the constraints of this study (one temperature independent parameter to describe a given binary mixture pair). The Henry's law constant of aqueous systems, e.g., is satisfactorily represented only by molecular simulation, whereas the cryogenic VLE of H_2 mixtures could not be calculated with the GERG-2008 EOS. In this regard, it would be desirable that H_2 mixtures receive more attention in empirical multiparameter EOS development. As expected, results from the Peng-Robinson EOS for the saturated liquid density deviate considerably. In summary, molecular modeling and simulation yields the best overall agreement with experimental data and, at the same time, is most versatile with respect to different thermodynamic properties and state points.

With the present molecular mixture model, a contribution to improving the availability of thermodynamic data for the upcoming hydrogen age was made. In principle, this model can be used to predict thermodynamic properties of this quinary mixture and its 25 subsystems due to pairwise additivity.

Acknowledgments

The authors gratefully acknowledge the Paderborn Center for Parallel Computing (PC^2) for the generous allocation of computer time on the OCuLUS cluster and computational support by the High Performance Computing Center Stuttgart (HLRS) under the grant MMHBF2. The authors wish to thank Denis Šarić for helping with the molecular simulations and Dr.-Ing. Christoph Held for his assistance during the PC-SAFT EOS calculations. The present

research was conducted under the auspices of the Boltzmann-Zuse Society of Computational Molecular Engineering (BZS).

Supporting Information

Supporting Information Available:

- Predictive mixture data for H_2 + O_2.
- Additional VLE data.
- VLE results for H_2 mixtures from the GERG-2008 EOS.
- Results from the PC-SAFT and the Peng-Robinson EOS for the Henry's law constant.
- Numerical molecular simulation data.

References

(1) United Nations Framework Convention on Climate Change, *The Paris Agreement*. 2015; `http://unfccc.int/files/essential_background/convention/application/pdf/english_paris_agreement.pdf` (accessed July 7, 2017).

(2) Klare, M. *Resource Wars: The New Landscape of Global Conflict*; Henry Holt and Company, New York, 2002.

(3) Bannon, I.; Collier, P. *Natural Resources and Violent Conflict: Options and Actions*; World Bank Publications, Washington, 2003.

(4) Bertuccioli, L.; Chan, A.; Hart, D.; Lehner, F.; Madden, B.; Standen, E. *Study on development of water electrolysis in the EU*. 2014; Final report in fuel cells and hydrogen joint undertaking.

(5) Edwards, P. P.; Kuznetsov, V. L.; David, W. I. F.; Brandon, N. P. Hydrogen and fuel cells: towards a sustainable energy future. *Energy Pol.* **2008**, *36*, 4356–4362.

(6) Momirlan, M.; Veziroglu, T. N. The properties of hydrogen as fuel tomorrow in sustainable energy system for a cleaner planet. *Int. J. Hydrogen Energy* **2005**, *30*, 795–802.

(7) Center for Transportation and the Environment, *International Fuel Cell Bus Workshop Report*. 2016; `http://www.cte.tv/wp-content/uploads/2016/12/FCBW-Report.pdf` (accessed July 7, 2017).

(8) Alstom Holding, *Alstom's hydrogen train Coradia iLint first successful run at 80 km/h*. 2017; `http://www.alstom.com/press-centre/2017/03/alstoms-hydrogen-train-coradia-ilint-first-successful-run-at-80-kmh` (accessed July 7, 2017).

(9) Dunn, S. Hydrogen futures: toward a sustainable energy system. *Int. J. Hydrogen Energy* **2002**, *27*, 235–264.

(10) Götz, M.; Lefebvre, J.; Mörs, F.; Koch, A. M.; Graf, F.; Bajohr, S.; Reimert, R.; Kolb, T. Renewable Power-to-Gas: A technological and economic review. *Renew. Energy* **2016**, *85*, 1371–1390.

(11) Stoll, J.; Vrabec, J.; Hasse, H. Vapor–liquid equilibria of mixtures containing nitrogen, oxygen, carbon dioxide, and ethane. *AIChE J.* **2003**, *49*, 2187–2198.

(12) Vrabec, J.; Stoll, J.; Hasse, H. Molecular models of unlike interactions in fluid mixtures. *Mol. Sim.* **2005**, *31*, 215–221.

(13) Huang, Y.-L.; Vrabec, J.; Hasse, H. Prediction of ternary vapor–liquid equilibria for 33 systems by molecular simulation. *Fluid Phase Equilib.* **2009**, *287*, 62–69.

(14) Eckl, B.; Schnabel, T.; Vrabec, J.; Wendland, M.; Hasse, H. Thermophysical properties of dry and humid air by molecular simulation including dew point calculations with the Mollier ensemble. *Ind. Eng. Chem. Res.* **2009**, *48*, 10110–10119.

(15) Vrabec, J.; Kedia, G. K.; Buchhauser, U.; Meyer-Pittroff, R.; Hasse, H. Thermodynamic models for vapor–liquid equilibria of nitrogen+ oxygen+ carbon dioxide at low temperatures. *Cryogenics* **2009**, *49*, 72–79.

(16) Tenorio, M.-J.; Parrott, A. J.; Calladine, J. A.; Sanchez-Vicente, Y.; Cresswell, A. J.; Graham, R. S.; Drage, T. C.; Poliakoff, M.; Ke, J.; George, M. W. Measurement of the vapour–liquid equilibrium of binary and ternary mixtures of CO_2, N_2 and H_2, systems which are of relevance to CCS technology. *Int. J. Greenh. Gas Control* **2015**, *41*, 68–81.

(17) Cresswell, A. J.; Wheatley, R. J.; Wilkinson, R. D.; Graham, R. S. Molecular simulation of the thermophysical properties and phase behaviour of impure CO_2 relevant to CCS. *Farad. Discuss.* **2016**, *192*, 415–436.

(18) Diamantonis, N. I.; Economou, I. G. Evaluation of statistical associating fluid theory (SAFT) and perturbed chain-SAFT equations of state for the calculation of thermodynamic derivative properties of fluids related to carbon capture and sequestration. *Energy Fuels* **2011**, *25*, 3334–3343.

(19) Diamantonis, N. I.; Boulougouris, G. C.; Mansoor, E.; Tsangaris, D. M.; Economou, I. G. Evaluation of cubic, SAFT, and PC-SAFT equations of state for the vapor–liquid equilibrium modeling of CO_2 mixtures with other gases. *Ind. Eng. Chem. Res.* **2013**, *52*, 3933–3942.

(20) Sun, R.; Lai, S.; Dubessy, J. Calculations of vapor–liquid equilibria of the H_2O-N_2 and H_2O-H_2 systems with improved SAFT-LJ EOS. *Fluid Phase Equilib.* **2015**, *390*, 23–33.

(21) Kunz, O.; Wagner, W. The GERG-2008 wide-range equation of state for natural gases and other mixtures: an expansion of GERG-2004. *J. Chem. Eng. Data* **2012**, *57*, 3032–3091.

(22) Gernert, J.; Span, R. EOS–CG: A Helmholtz energy mixture model for humid gases and CCS mixtures. *J. Chem. Thermodyn.* **2016**, *93*, 274–293.

(23) Allen, M. P.; Tildesley, D. J. *Computer simulation of liquids*; Oxford University Press, Oxford, 1989.

(24) Vrabec, J.; Stoll, J.; Hasse, H. A set of molecular models for symmetric quadrupolar fluids. *J. Phys. Chem. B* **2001**, *105*, 12126–12133.

(25) Windmann, T.; Linnemann, M.; Vrabec, J. Fluid Phase Behavior of Nitrogen + Acetone and Oxygen + Acetone by Molecular Simulation, Experiment and the Peng–Robinson Equation of State. *J. Chem. Eng. Data* **2013**, *59*, 28–38.

(26) Elts, E.; Windmann, T.; Staak, D.; Vrabec, J. Fluid phase behavior from molecular simulation: Hydrazine, Monomethylhydrazine, Dimethylhydrazine and binary mixtures containing these compounds. *Fluid Phase Equilib.* **2012**, *322*, 79–91.

(27) Huang, Y.-L.; Miroshnichenko, S.; Hasse, H.; Vrabec, J. Henry's law constant from molecular simulation: a systematic study of 95 systems. *Int. J. Thermophys.* **2009**, *30*, 1791–1810.

(28) Vrabec, J.; Huang, Y.-L.; Hasse, H. Molecular models for 267 binary mixtures validated by vapor–liquid equilibria: A systematic approach. *Fluid Phase Equilib.* **2009**, *279*, 120–135.

(29) Abascal, J. L. F.; Vega, C. A general purpose model for the condensed phases of water: TIP4P/2005. *J. Chem. Phys.* **2005**, *123*, 234505.

(30) Vega, C.; Abascal, J. L. F. Simulating water with rigid non-polarizable models: a general perspective. *Phys. Chem. Chem. Phys.* **2011**, *13*, 19663–19688.

(31) Shvab, I.; Sadus, R. J. Atomistic water models: Aqueous thermodynamic properties from ambient to supercritical conditions. *Fluid Phase Equilib.* **2016**, *407*, 7–30.

(32) Köster, A.; Spura, T.; Rutkai, G.; Kessler, J.; Wiebeler, H.; Vrabec, J.; Kühne, T. D. Assessing the accuracy of improved force-matched water models derived from Ab initio molecular dynamics simulations. *J. Comput. Chem.* **2016**, *37*, 1828–1838.

(33) Nagashima, H.; Tsuda, S.; Tsuboi, N.; Koshi, M.; Hayashi, K.; Tokumasu, T. An analysis of quantum effects on the thermodynamic properties of cryogenic hydrogen using the path integral method. *J. Chem. Phys.* **2014**, *140*, 134506.

(34) Leachman, J. W.; Jacobsen, R. T.; Penoncello, S. G.; Lemmon, E. W. Fundamental equations of state for parahydrogen, normal hydrogen, and orthohydrogen. *J. Phys. Chem. Ref. Data* **2009**, *38*, 721–748.

(35) Hirschfelder, J.; Curtiss, C. F.; Bird, R. B. *Molecular theory of gases and liquids*; John Wiley & Sons, New York, 1964.

(36) Marx, D.; Nielaba, P. Path-integral Monte Carlo techniques for rotational motion in two dimensions: Quenched, annealed, and no-spin quantum-statistical averages. *Phys. Rev. A* **1992**, *45*, 8968–8971.

(37) Buch, V. Path integral simulations of mixed *para*-D_2 and *ortho*-D_2 clusters: The orientational effects. *J. Chem. Phys.* **1994**, *100*, 7610–7629.

(38) Darkrim, F.; Levesque, D. Monte Carlo simulations of hydrogen adsorption in single-walled carbon nanotubes. *J. Chem. Phys.* **1998**, *109*, 4981–4984.

(39) Belof, J. L.; Stern, A. C.; Space, B. An accurate and transferable intermolecular diatomic hydrogen potential for condensed phase simulation. *J. Chem. Theory Comput.* **2008**, *4*, 1332–1337.

(40) Engin, C.; Vrabec, J.; Hasse, H. On the difference between a point multipole and an equivalent linear arrangement of point charges in force field models for vapour–liquid equilibria; partial charge based models for 59 real fluids. *Mol. Phys.* **2011**, *109*, 1975–1982.

(41) Schnabel, T.; Vrabec, J.; Hasse, H. Unlike Lennard–Jones parameters for vapor–liquid equilibria. *J. Mol. Liq.* **2007**, *135*, 170–178.

(42) Frenkel, D.; Smit, B. *Understanding Molecular Simulation: From Algorithms to Applications*; Academic Press, San Diego, 2002.

(43) Deublein, S.; Eckl, B.; Stoll, J.; Lishchuk, S. V.; Guevara-Carrion, G.; Glass, C. W.; Merker, T.; Bernreuther, M.; Hasse, H.; Vrabec, J. *ms*2: A molecular simulation tool for thermodynamic properties. *Comput. Phys. Commun.* **2011**, *182*, 2350–2367.

(44) Glass, C. W.; Reiser, S.; Rutkai, G.; Deublein, S.; Köster, A.; Guevara-Carrion, G.; Wafai, A.; Horsch, M.; Bernreuther, M.; Windmann, T.; Hasse, H.; Vrabec, J. *ms*2: A molecular simulation tool for thermodynamic properties, new version release. *Comput. Phys. Commun.* **2014**, *185*, 3302–3306.

(45) Rutkai, G.; Köster, A.; Guevara-Carrion, G.; Janzen, T.; Schappals, M.; Glass, C. W.; Bernreuther, M.; Wafai, A.; Stephan, S.; Kohns, M.; Reiser, S.; Deublein, S.; Horsch, M.; Hasse, H.; Vrabec, J. *ms*2: A molecular simulation tool for thermodynamic properties, release 3.0. *Comput. Phys. Commun.* **2017**, *221*, 343–351.

(46) Lustig, R. Angle-average for the powers of the distance between two separated vectors. *Mol. Phys.* **1988**, *65*, 175–179.

(47) Flyvbjerg, H.; Petersen, H. G. Error estimates on averages of correlated data. *J. Chem. Phys.* **1989**, *91*, 461–466.

(48) Vrabec, J.; Hasse, H. Grand Equilibrium: vapour-liquid equilibria by a new molecular simulation method. *Mol. Phys.* **2002**, *100*, 3375–3383.

(49) Widom, B. Some topics in the theory of fluids. *J. Chem. Phys.* **1963**, *39*, 2808–2812.

(50) Shing, K. S.; Gubbins, K. E.; Lucas, K. Henry constants in non-ideal fluid mixtures: computer simulation and theory. *Mol. Phys.* **1988**, *65*, 1235–1252.

(51) Gross, J.; Sadowski, G. Perturbed-chain SAFT: An equation of state based on a perturbation theory for chain molecules. *Ind. Eng. Chem. Res.* **2001**, *40*, 1244–1260.

(52) Gross, J.; Sadowski, G. Application of the perturbed-chain SAFT equation of state to associating systems. *Ind. Eng. Chem. Res.* **2002**, *41*, 5510–5515.

(53) Gross, J.; Vrabec, J. An equation-of-state contribution for polar components: Dipolar molecules. *AIChE J.* **2006**, *52*, 1194–1204.

(54) Gross, J. An equation-of-state contribution for polar components: Quadrupolar molecules. *AIChE J.* **2005**, *51*, 2556–2568.

(55) Vrabec, J.; Gross, J. Vapor- liquid equilibria simulation and an equation of state contribution for dipole- quadrupole interactions. *J. Phys. Chem. B* **2008**, *112*, 51–60.

(56) Kleiner, M.; Sadowski, G. Modeling of polar systems using PCP-SAFT: an approach to account for induced-association interactions. *J. Phys. Chem. C* **2007**, *111*, 15544–15553.

(57) Tumakaka, F.; Gross, J.; Sadowski, G. Thermodynamic modeling of complex systems using PC-SAFT. *Fluid Phase Equilib.* **2005**, *228*, 89–98.

(58) Aasen, A.; Hammer, M.; Skaugen, G.; Jakobsen, J. P.; Wilhelmsen, Ø. Thermodynamic models to accurately describe the *PVTxy*-behavior of water / carbon dioxide mixtures. *Fluid Phase Equilib.* **2017**, *442*, 125–139.

(59) Stavrou, M.; Lampe, M.; Bardow, A.; Gross, J. Continuous molecular targeting–computer-aided molecular design (CoMT–CAMD) for simultaneous process and solvent design for CO_2 capture. *Ind. Eng. Chem. Res.* **2014**, *53*, 18029–18041.

(60) Kiesow, K.; Tumakaka, F.; Sadowski, G. Experimental investigation and prediction of oiling out during crystallization process. *J. Cryst. Growth* **2008**, *310*, 4163–4168.

(61) Vinš, V.; Hrubỳ, J. Solubility of nitrogen in one-component refrigerants: Prediction by PC-SAFT EoS and a correlation of Henry's law constants. *Int. J. Refrig.* **2011**, *34*, 2109–2117.

(62) Peng, D.-Y.; Robinson, D. B. A new two-constant equation of state. *Ind. Eng. Chem. Fundam.* **1976**, *15*, 59–64.

(63) Lopez-Echeverry, J. S.; Reif-Acherman, S.; Araujo-Lopez, E. Peng-Robinson equation of state: 40 years through cubics. *Fluid Phase Equilib.* **2017**, *447*, 39–71.

(64) Soave, G. Equilibrium constants from a modified Redlich-Kwong equation of state. *Chem. Eng. Sci.* **1972**, *27*, 1197–1203.

(65) Mathias, P. M.; Copeman, T. W. Extension of the Peng-Robinson equation of state to complex mixtures: evaluation of the various forms of the local composition concept. *Fluid Phase Equilib.* **1983**, *13*, 91–108.

(66) Stryjek, R.; Vera, J. H. PRSV: An improved PengRobinson equation of state for pure compounds and mixtures. *Can. J. Chem. Eng.* **1986**, *64*, 323–333.

(67) Twu, C. H.; Coon, J. E.; Cunningham, J. R. A new generalized alpha function for a cubic equation of state Part 1. Peng-Robinson equation. *Fluid Phase Equilib.* **1995**, *105*, 49–59.

(68) Dortmund Data Base. 2015; version 7.3.0.459.

(69) Sandler, S. I. *Chemical, biochemical, and engineering thermodynamics*; John Wiley & Sons, Hoboken, 2006.

(70) Wagner, W.; Pruß, A. The IAPWS formulation 1995 for the thermodynamic properties of ordinary water substance for general and scientific use. *J. Phys. Chem. Ref. Data* **2002**, *31*, 387–535.

(71) Span, R.; Wagner, W. A new equation of state for carbon dioxide covering the fluid region from the triple-point temperature to 1100 K at pressures up to 800 MPa. *J. Phys. Chem. Ref. Data* **1996**, *25*, 1509–1596.

(72) Eubanks, L. S. Vapor-Liquid equilibria in the system Hydrogen-Nitrogen-Carbon monoxide. Ph.D. thesis, Rice University, 1957.

(73) Akers, W. W.; Eubanks, L. S. Vapor-Liquid Equilibria in the System Hydrogen-Nitrogen-Carbon Monoxide. *Adv. Cryog. Eng.* **1960**, *3*, 275–293.

(74) Streett, W. B.; Calado, J. C. G. Liquid-vapour equilibrium for hydrogen + nitrogen at temperatures from 63 to 110 K and pressures to 57 MPa. *J. Chem. Thermodyn.* **1978**, *10*, 1089–1100.

(75) Xiao, J.; Liu, K. Measurement and correlation of vapor - liquid equilibrium data in H2 - N2 - Ar system. *J. Chem. Eng. (China)* **1990**, *8*, 8–12.

(76) Span, R.; Lemmon, E. W.; Jacobsen, R. T.; Wagner, W.; Yokozeki, A. A reference equation of state for the thermodynamic properties of nitrogen for temperatures from 63.151 to 1000 K and pressures to 2200 MPa. *J. Phys. Chem. Ref. Data* **2000**, *29*, 1361–1433.

(77) Calado, J. C. G.; Streett, W. B. Liquid-vapor equilibrium in the system H_2 + Ar at temperatures from 83 to 141 K and pressures to 52 MPa. *Fluid Phase Equilib.* **1979**, *2*, 275–282.

(78) Ostronov, M. G.; Shatskaya, L. V.; Finyagina, R. A.; Brodskaya, L. F.; Zhirnova, N. A. Gas-Liquid Phase Equilibrium in the Argon-Hydrogen System at Intermediate Pressures. *Russ. J. Phys. Chem.* **1977**, *51*, 1407–1409.

(79) Volk, H.; Halsey Jr., G. D. Solubility of hydrogen and deuterium in liquid argon. *J. Chem. Phys.* **1960**, *33*, 1132–1139.

(80) Mullins, J. C.; Ziegler, W. T. Phase equilibria in the argon-helium and argon-hydrogen systems from 68 to 108 K and pressures to 120 atmospheres. *Adv. Cryog. Eng.* **1965**, *10*, 171–181.

(81) DeVaney, W.; Berryman, J. M.; Kao, P.-L.; Eakin, B. *High temperature VLE measurements for substitute gas components*. 1978; GPA Research Report RR-30.

(82) Gillespie, P. C.; Wilson, G. M. *Vapor-Liquid Equilibrium Data on Water-Substitute*

Gas Components:N_2-H_2O,H_2-H_2O,CO-H_2O,H_2-CO-H_2O, and H_2S-H_2O. 1982; GPA Research Report RR-48.

(83) Ipat'ev, V. V.; Teodorovich, V. P. Solubility of hydrogen in water under pressure at elevated temperatures. *Zhur. Obsh. Khim* **1934**, *4*, 395–397.

(84) Kling, G.; Maurer, G. The solubility of hydrogen in water and in 2-aminoethanol at temperatures between 323 K and 423 K and pressures up to 16 MPa. *J. Chem. Thermodyn.* **1991**, *23*, 531–541.

(85) Maslennikova, V. Y.; Goryunova, N. P.; Subbotina, L. A.; Tsiklis, D. S. The solubility of water in compressed hydrogen. *Russ. J. Phys. Chem.* **1976**, *50*, 240–243.

(86) Dodge, B. F. Isotherms and isobars for air separation studies. *Chem. Metall. Eng.* **1928**, *35*, 622.

(87) Baidakov, V. G.; Kaverin, A. M.; Andbaeva, V. N. The liquid-gas interface of oxygen-nitrogen solutions: 1. Surface tension. *Fluid Phase Equilib.* **2008**, *270*, 116–120.

(88) Maslennikova, V. Y.; Vdovina, N. A.; Tsiklis, D. S. The solubility of water in compressed nitrogen. *Russ. J. Phys. Chem.* **1971**, *45*, 1354.

(89) Maslennikova, V. Y. The solubility of nitrogen in water. *Trudy GIAP, Moscow* **1971**, *12*, 82–87.

(90) Saddington, A. W.; Krase, N. W. Vapor-Liquid Equilibria in the System Nitrogen-Water. *J. Am. Chem. Soc.* **1934**, *56*, 353–361.

(91) Japas, M. L.; Franck, E. U. High Pressure Phase Equilibria and PVT-Data. of the Water-Nitrogen System to 673 K and 250 MPa. *Ber. Bunsenges. Phys. Chem.* **1985**, *89*, 793–800.

(92) Narinskii, G. B. Liquid-vapor equilibrium in argon-nitrogen system. I. Experimental data and their verification. *Russ. J. Phys. Chem.* **1966**, *40*, 1093–1096.

(93) Liu, K.; Wang, W. VLE Measurement and Correlation of N_2-Ar-CH_4 System at 122.89 K. *J. Chem. Eng. (China)* **1988**, *16*, 58–63.

(94) Bourbo, P.; Ischkin, I. Study of the vapor-liquid equilibrium of the system argon-oxygen. *Phys. Z. Sowjetunion* **1936**, *10*, 271–291.

(95) Baba-Ahmed, A. Appareillage pour l'étude des équilibre liquide–vapeur dans le domaine cryogénique conception et développement. Ph.D. thesis, Ecole des Mines de Paris, 1999.

(96) Narinskii, G. B. Investigation of the liquid-vapor equilibrium in the oxygen-argon system. *Kislorod* **1957**, *10*, 9–16.

(97) Bennett, C. O.; Dodge, B. F. Compressibilities of mixtures of hydrogen and nitrogen above 1000 atmospheres. *Ind. Eng. Chem.* **1952**, *44*, 180–185.

(98) Verschoyle, T. T. H. Isotherms of Hydrogen, of Nitrogen, and of Hydrogen-Nitrogen Mixtures, at 0° and 20° C., up to a Pressure of 200 Atmospheres. *Proc. R. Soc. A* **1926**, *111*, 552–576.

(99) Zandbergen, P.; Beenakker, J. J. M. Experimental determination of the volume change on mixing for gaseous N_2-H_2, Ar-H_2 and Ar-N_2 between 170 and 292° K up to 100 ATM. *Physica* **1967**, *33*, 343–365.

(100) Kuenen, J. P.; Verschoyle, T.; van Urk, A. T. Isotherms of Diatomic Substances and their Binary Mixtures. XX. The Critical Curve of Oxygen - Nitrogen Mixtures, the Critical Phenomena and some Isotherms of Two Mixtures of 50% and 75% by Volume of Oxygen in the Neighborhood of the Critical Region. *Proc. R. Acad.* **1922**, *22*, 49–64.

(101) Palavra, A. M. Effect of pressure and temperature on excess properties in the system argon-nitrogen. M.Sc. thesis, Universidade Tecnica De Lisboa, 1979.

(102) Crain Jr, R. W.; Sonntag, R. E. *Advances in Cryogenic Engineering*; Springer, New York, 1966; pp 379–391.

(103) Masson, I.; Dolley, L. G. F. The Pressures of Gaseous Mixtures. *Proc. R. Soc. A* **1923**, *103*, 524–538.

(104) Fernández-Prini, R.; Alvarez, J. L.; Harvey, A. H. Henry's constants and vapor–liquid distribution constants for gaseous solutes in H_2O and D_2O at high temperatures. *J. Phys. Chem. Ref. Data* **2003**, *32*, 903–916.

(105) International Association for the Properties of Water and Steam, *Guideline on the Henry's Constant and Vapor-Liquid Distribution Constant for Gases in H_2O and D_2O at High Temperatures*. 2004.

(106) Morris, D. R.; Yang, L.; Giraudeau, F.; Sun, X.; Steward, F. R. Henry's law constant for hydrogen in natural water and deuterium in heavy water. *Phys. Chem. Chem. Phys.* **2001**, *3*, 1043–1046.

(107) Alvarez, J.; Fernández-Prini, R. A semiempirical procedure to describe the thermodynamics of dissolution of non-polar gases in water. *Fluid Phase Equilib.* **1991**, *66*, 309–326.

(108) Rettich, T. R.; Battino, R.; Wilhelm, E. Solubility of gases in liquids. XVI. Henry's law coefficients for nitrogen in water at 5 to 50° C. *J. Solution Chem.* **1984**, *13*, 335–348.

(109) Cosgrove, B. A.; Walkley, J. Solubilities of gases in H_2O and ^2H_2O. *J. Chromatogr. A* **1981**, *216*, 161–167.

(110) Alvarez, J.; Crovetto, R.; Fernández-Prini, R. The dissolution of N_2 and of H_2 in water from room temperature to 640 K. *Ber. Bunsenges. Phys. Chem.* **1988**, *92*, 935–940.

(111) Rettich, T. R.; Battino, R.; Wilhelm, E. Solubility of gases in liquids. 22. High-precision determination of Henry's law constants of oxygen in liquid water from T= 274 K to T= 328 K. *J. Chem. Thermodyn.* **2000**, *32*, 1145–1156.

(112) Benson, B. B.; Krause, D.; Peterson, M. A. The solubility and isotopic fractionation of gases in dilute aqueous solution. I. Oxygen. *J. Solution Chem.* **1979**, *8*, 655–690.

(113) Rettich, T. R.; Handa, Y. P.; Battino, R.; Wilhelm, E. Solubility of gases in liquids. 13. High-precision determination of Henry's constants for methane and ethane in liquid water at 275 to 328 K. *J. Phys. Chem.* **1981**, *85*, 3230–3237.

(114) Cramer, S. D. The solubility of oxygen in brines from 0 to 300° C. *Ind. Eng. Chem. Process Des. Dev.* **1980**, *19*, 300–305.

(115) Rettich, T. R.; Battino, R.; Wilhelm, E. Solubility of gases in liquids. 18. High-precision determination of Henry fugacities for argon in liquid water at 2 to 40° C. *J. Solution Chem.* **1992**, *21*, 987–1004.

(116) Krause, D.; Benson, B. B. The solubility and isotopic fractionation of gases in dilute aqueous solution. IIa. Solubilities of the noble gases. *J. Solution Chem.* **1989**, *18*, 823–873.

(117) Potter, R. W.; Clynne, M. A. The solubility of the noble gases He, Ne, Ar, Kr, and Xe in water up to the critical point. *J. Solution Chem.* **1978**, *7*, 837–844.

(118) Crovetto, R.; Fernández-Prini, R.; Japas, M. L. Solubilities of inert gases and methane in H_2O and in D_2O in the temperature range of 300 to 600 K. *J. Chem. Phys.* **1982**, *76*, 1077–1086.

(119) Fastovskii, V. G.; Petrovskii, Y. V. A study of the vapor-liquid equilibrium in the system oxygen-argon-nitrogen. *Zh. Fiz. Khim.* **1957**, *31*, 836–841.

(120) Lemmon, E. W.; Jacobsen, R. T.; Penoncello, S. G.; Friend, D. G. Thermodynamic properties of air and mixtures of nitrogen, argon, and oxygen from 60 to 2000 K at pressures to 2000 MPa. *J. Phys. Chem. Ref. Data.* **2000**, *29*, 331–385.

(121) Holborn, L.; Schultze, H. Über die Druckwage und die Isothermen von Luft, Argon und Helium zwischen 0 und 200° C. *Ann. Phys.* **1915**, *352*, 1089–1111.

(122) Kozlov, A. Experimental investigation of the specific volumes of air in the 20-600°C temperature range and 20-700 bar pressure range. Ph.D. thesis, Moscow, 1968.

(123) Diller, D. E.; Aragon, A. S.; Laesecke, A. Measurements of the viscosity of compressed liquid air at temperatures between 70 and 130 K. *Cryogenics* **1991**, *31*, 1070–1072.

(124) Japas, M. L.; Franck, E. U. High Pressure Phase Equilibria and PVT-Data of the Water-Oxygen System Including Water-Air to 673 K and 250 MPa. *Ber. Bunsenges. Phys. Chem.* **1985**, *89*, 1268–1275.

(125) Ulbig, P.; Trusler, M.; Wendland, M.; Wöll, O.; Nieto de Castro, C. A. *Summary report on experimental results for thermodynamic and transport properties, AA-CAES, Deliverable Report D4.1*. 2005.

TOC Graphic

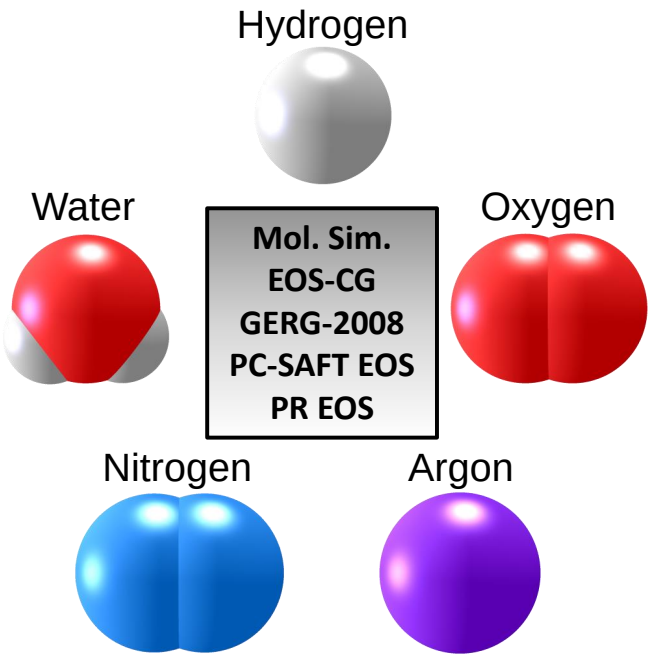
Hydrogen
Water
Oxygen
Mol. Sim.
EOS-CG
GERG-2008
PC-SAFT EOS
PR EOS
Nitrogen
Argon

TOC Graphic

Supporting information for:

Molecular models for the hydrogen age:

Hydrogen, nitrogen, oxygen, argon and water

Andreas Köster,[†] Monika Thol,[‡] and Jadran Vrabec[*,†]

[†]*Lehrstuhl für Thermodynamik und Energietechnik, Universität Paderborn, 33098 Paderborn, Germany*

[‡]*Lehrstuhl für Thermodynamik, Ruhr-Universität Bochum, 44801 Bochum, Germany*

E-mail: jadran.vrabec@upb.de

Phone: +49-5251 60-2421. Fax: +49 5251 60-3522

Abstract

This supporting information contains predictive mixture data for H_2 + O_2, additional VLE data for mixtures discussed in the main manuscript, VLE results for H_2 mixtures from the GERG-2008 EOS, results from the PC-SAFT and the Peng-Robinson EOS for the Henry's law constant and all molecular simulation data with the associated statistical uncertainty in numerical form. The confidence level for the reported data is 68.3 % ($\pm$1 standard deviation).

Contents

1 Predictive mixture data for $H_2 + O_2$

No experimental data were available for this mixture so that the results shown in Fig. S1 are strictly predictive (no binary interaction parameter was adjusted).

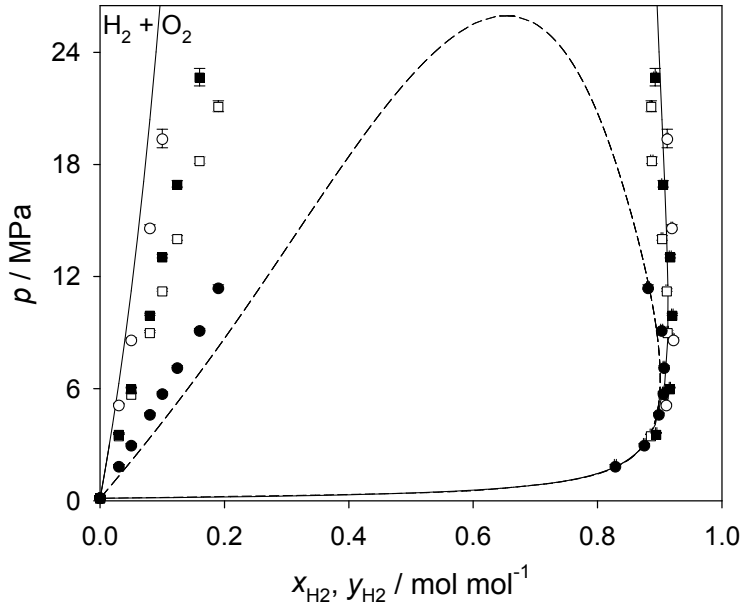

Figure S1: Isothermal fluid phase diagram of the binary mixture $H_2 + O_2$: (○, □) Molecular simulation results obtained with the present H_2 force field or (●, ■) with the H_2 force field of Marx and Nielaba[S1], (—) Peng-Robinson EOS and (- -) PC-SAFT EOS. For comparison, (□) and (■) depict molecular simulation data with binary interaction parameters of the chemically similar mixture $H_2 + N_2$, cf. Table 4 in the main manuscript. Statistical uncertainties of the molecular simulation data are only shown if they exceed symbol size.

2 Additional VLE data

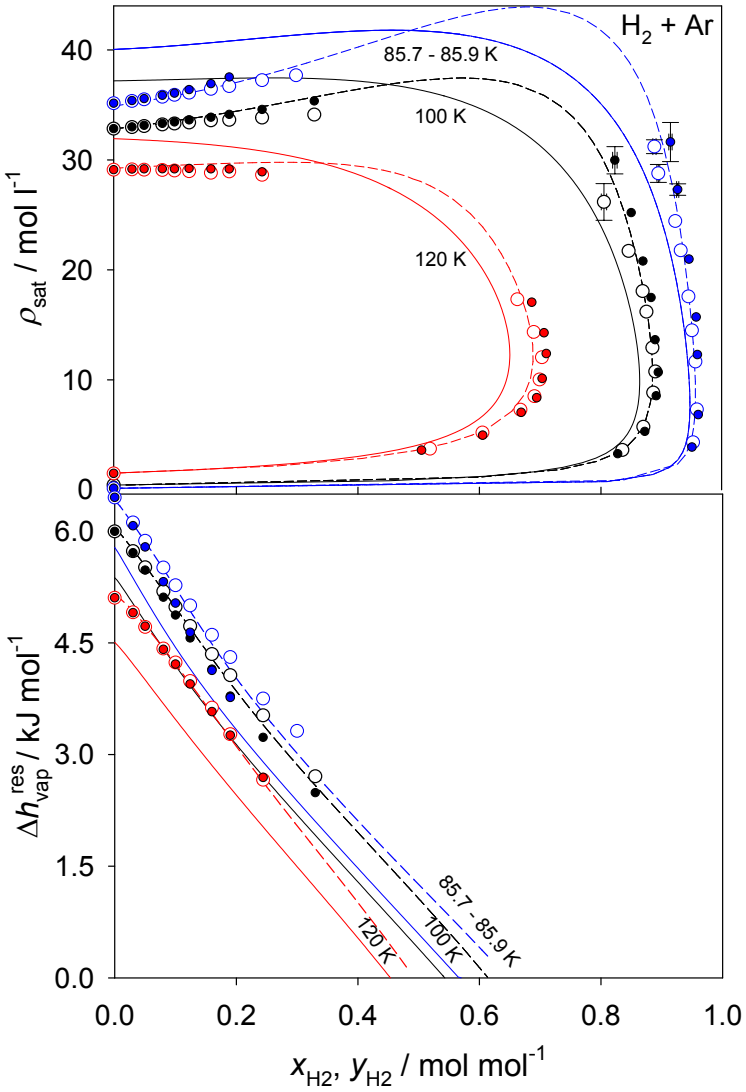

Figure S2: Isothermal saturated densities ρ_{sat} (top) and residual enthalpy of vaporization $h_{\mathrm{vap}}^{\mathrm{res}}$ (bottom) of the binary mixture H_2 + Ar: (○) Molecular simulation results obtained with the present H_2 force field or (●) with the H_2 force field of Marx and Nielaba[S1], (—) Peng-Robinson EOS and (- -) PC-SAFT EOS. Statistical uncertainties of the molecular simulation data are only shown if they exceed symbol size.

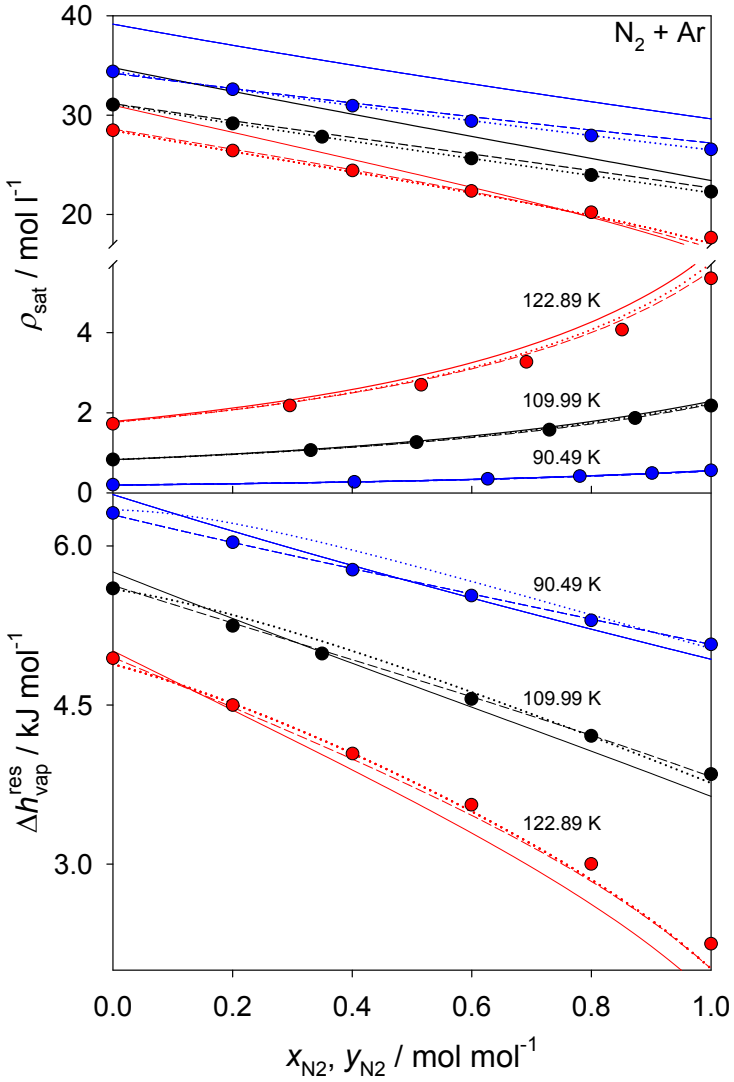

Figure S3: Isothermal saturated densities ρ_{sat} (top) and residual enthalpy of vaporization $h_{\text{vap}}^{\text{res}}$ (bottom) of the binary mixture N_2 + Ar: (•) Molecular simulation results, (—) Peng-Robinson EOS, (- -) PC-SAFT EOS and (· · ·) EOS-CG.

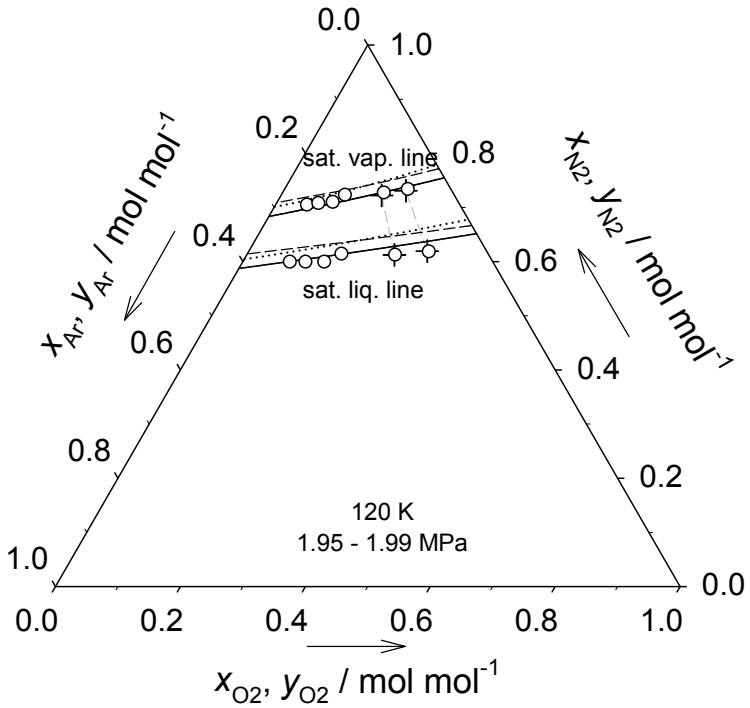

Figure S4: Fluid phase diagram of the ternary system N_2 + O_2 + Ar at 120 K and 1.95 to 1.99 MPa: (∘) Molecular simulation results, (—) Peng-Robinson EOS, (- -) PC-SAFT EOS, (· · ·) EOS-CG and (+) experimental literature data[S2].

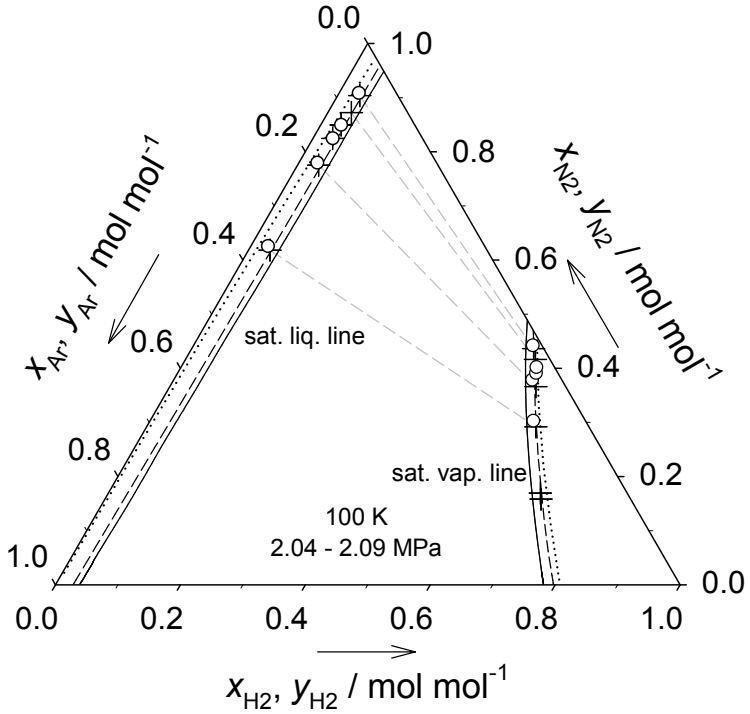

Figure S5: Fluid phase diagram of the ternary system H_2 + N_2 + Ar at 100 K and 2.04 to 2.09 MPa: (○) Molecular simulation results, (—) Peng-Robinson EOS, (- -) PC-SAFT EOS, (· · ·) GERG-2008 EOS and (+) experimental literature data[S3].

3 VLE results for H_2 mixtures from the GERG-2008 EOS

In Fig. S6 the GERG-2008 EOS was used to calculate the phase envelope of H_2 mixtures. It can be seen that in some cases a false liquid-liquid equilibrium is predicted (bottom). In other cases, the vapor pressure is strongly overestimated. However, cryogenic H_2 mixtures were not the main focus during the development of the GERG-2008 EOS and its normal range of validity in temperature is specified as 90 to 450 K[S4], which means that the lowest isotherm is an extrapolation.

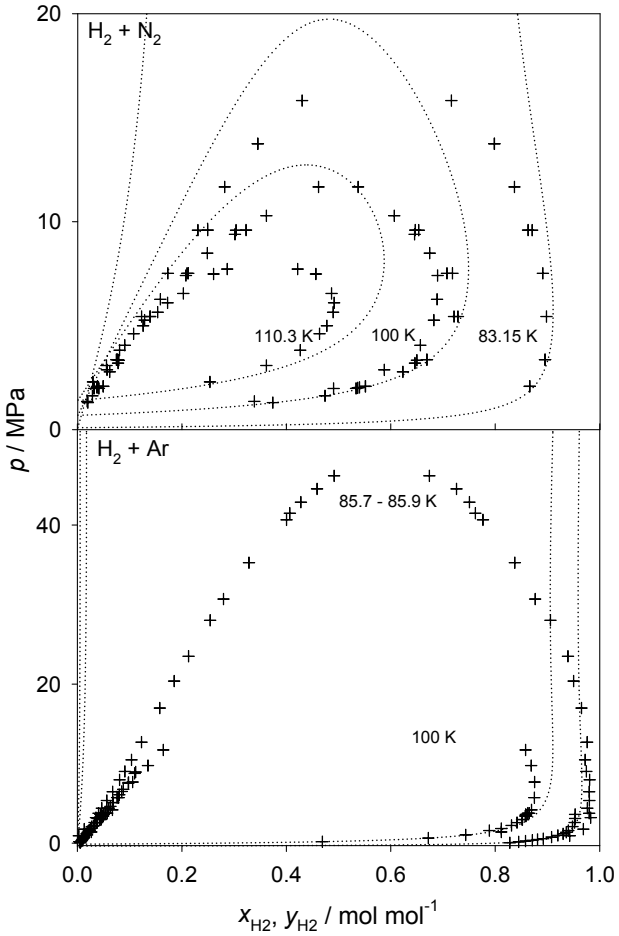

Figure S6: Isothermal fluid phase diagram of the binary mixtures H_2 + N_2 (top) and H_2 + Ar (bottom): (+) Experimental literature data[S3,S5–S11] and (· · ·) GERG-2008 EOS[S4].

4 Henry's law constant from the PC-SAFT and the Peng-Robinson EOS

As discussed in the main manuscript, both the PC-SAFT and the Peng-Robinson EOS fail to reproduce the Henry's law constant of H_2, N_2, O_2 and Ar in H_2O qualitatively, cf. Fig. S7. A single temperature independent binary interaction parameter was used for these calculations, cf. Table 4 in the main manuscript.

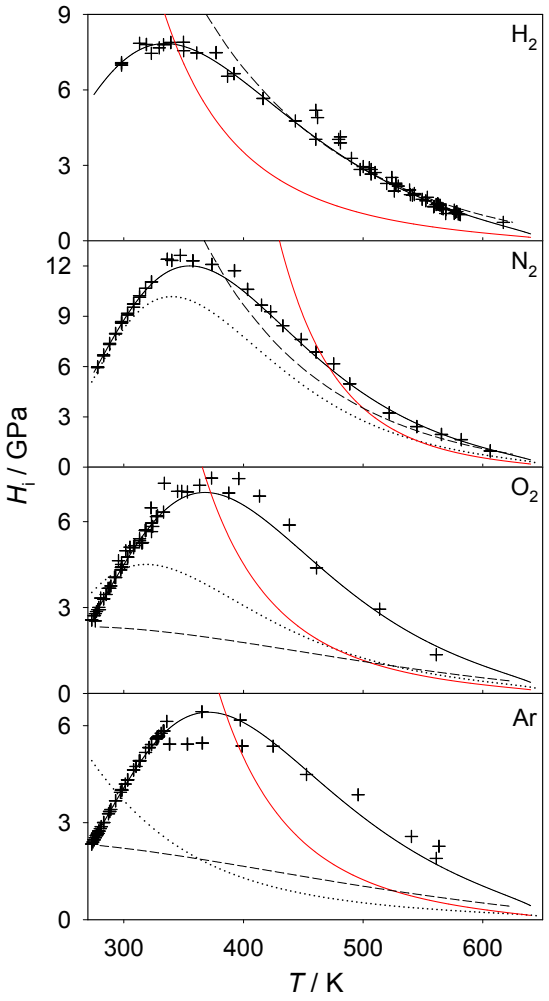

Figure S7: Henry's law constant of H_2, N_2, O_2 and Ar in H_2O (from top to bottom): (—, black) official IAPWS guideline[S12,S13], (—, red) Peng-Robinson EOS, (- -) PC-SAFT EOS, (···) EOS-CG and (+) experimental literature data (H_2 [S14,S15]; N_2 [S15–S18]; O_2 [S19–S22]; Ar [S23–S26]).

5 Numerical molecular simulation data

5.1 Binary mixtures

5.1.1 Hydrogen + nitrogen

Table S1: Homogeneous density data from molecular simulation for the equimolar mixture H_2 + N_2 using the present as well as the H_2 force field of Marx and Nielaba[S1]. Statistical uncertainties are denoted by δ.

T	p	$\rho_{\mathrm{H2,present}}$	$\delta\rho_{\mathrm{H2,present}}$	$\rho_{\mathrm{H2,Marx}}$	$\delta\rho_{\mathrm{H2,Marx}}$
K	MPa	mol/l	mol/l	mol/l	mol/l
273.15	4.667	2.0155	0.0002	2.0194	0.0002
273.15	5.642	2.4250	0.0002	2.4309	0.0002
273.15	8.082	3.4288	0.0003	3.4408	0.0003
273.15	10.530	4.4053	0.0005	4.4257	0.0005
273.15	12.979	5.3496	0.0006	5.3785	0.0006
273.15	14.938	6.0814	0.0007	6.1189	0.0007
273.15	16.897	6.7892	0.0008	6.8354	0.0008
273.15	18.858	7.4760	0.0009	7.5344	0.0009
273.15	19.838	7.812	0.001	7.8738	0.0008
273.15	20.818	8.1423	0.0009	8.207	0.001
323.13	101.125	20.956	0.002	21.279	0.002
323.13	153.849	25.587	0.002	26.009	0.002
323.13	205.233	28.817	0.002	29.303	0.002
323.13	252.193	31.138	0.002	31.672	0.002
323.13	302.878	33.209	0.002	33.785	0.002
373.12	100.861	19.087	0.002	19.348	0.002
373.12	153.755	23.735	0.002	24.096	0.002
373.12	202.721	26.879	0.002	27.303	0.002
373.12	252.448	29.405	0.002	29.883	0.002
373.12	304.578	31.588	0.002	32.105	0.002

Table S2: Vapor-liquid equilibrium data from molecular simulation for H_2 + N_2 using the present H_2 force field. Statistical uncertainties are denoted by δ.

T	p	δp	x_{H2}	y_{H2}	δy_{H2}	ρ_{liq}	$\delta\rho_{liq}$	ρ_{vap}	$\delta\rho_{vap}$	Δh_v^{res}	$\delta\Delta h_v^{res}$
K	MPa	MPa	mol/mol	mol/mol	mol/mol	mol/l	mol/l	mol/l	mol/l	kJ/mol	kJ/mol
83.15	0.196	0.001	0.00	0.000	0.000	27.895	0.005	0.302	0.002	5.399	0.001
83.15	1.327	0.005	0.03	0.816	0.002	28.067	0.005	2.010	0.007	5.208	0.001
83.15	2.09	0.01	0.05	0.862	0.002	28.182	0.006	3.17	0.02	5.046	0.002
83.15	3.28	0.02	0.08	0.890	0.002	28.382	0.006	5.02	0.03	4.803	0.002
83.15	4.01	0.03	0.10	0.900	0.002	28.511	0.007	6.13	0.04	4.649	0.003
83.15	5.06	0.05	0.12	0.903	0.002	28.710	0.008	7.77	0.07	4.450	0.003
83.15	6.59	0.07	0.16	0.900	0.003	28.994	0.005	10.2	0.1	4.147	0.004
83.15	7.9	0.1	0.19	0.892	0.003	29.223	0.005	12.3	0.2	3.88	0.01
83.15	10.4	0.2	0.24	0.863	0.005	29.681	0.008	16.1	0.3	3.38	0.01
83.15	14.1	0.4	0.33	0.833	0.006	30.16	0.03	21.0	0.6	2.64	0.02
100	0.794	0.003	0.00	0.000	0.000	24.662	0.008	1.146	0.004	4.554	0.002
100	1.818	0.005	0.03	0.479	0.002	24.717	0.007	2.526	0.007	4.402	0.003
100	2.51	0.01	0.05	0.583	0.002	24.80	0.01	3.47	0.01	4.268	0.004
100	3.51	0.02	0.08	0.661	0.002	24.84	0.01	4.82	0.02	4.05	0.01
100	4.19	0.02	0.10	0.687	0.002	24.91	0.01	5.78	0.03	3.90	0.01
100	5.13	0.03	0.12	0.699	0.003	25.08	0.01	7.16	0.04	3.68	0.01
100	6.42	0.04	0.16	0.708	0.003	25.239	0.009	9.08	0.06	3.38	0.01
100	8.39	0.05	0.24	0.717	0.003	24.69	0.01	11.85	0.07	2.73	0.01
100	10.20	0.07	0.33	0.695	0.004	24.04	0.05	14.6	0.1	2.02	0.02
110.3	1.512	0.005	0.00	0.000	0.000	22.21	0.01	2.243	0.007	3.813	0.004
110.3	2.44	0.01	0.03	0.279	0.002	22.24	0.01	3.50	0.01	3.66	0.01
110.3	3.05	0.01	0.05	0.370	0.002	22.13	0.01	4.32	0.01	3.51	0.01
110.3	3.89	0.01	0.08	0.453	0.002	22.05	0.01	5.49	0.02	3.30	0.01
110.3	4.65	0.02	0.10	0.478	0.003	22.29	0.01	6.69	0.03	3.12	0.01
110.3	5.24	0.02	0.12	0.517	0.003	22.13	0.02	7.41	0.03	2.97	0.01
110.3	6.04	0.03	0.16	0.527	0.003	21.61	0.02	8.71	0.04	2.61	0.01
110.3	6.82	0.03	0.19	0.526	0.004	21.46	0.02	10.11	0.05	2.31	0.02

Table S3: Vapor-liquid equilibrium data from molecular simulation for H_2 + N_2 using the H_2 force field of Marx and Nielaba[S1]. Statistical uncertainties are denoted by δ.

T	p	δp	x_{H2}	y_{H2}	δy_{H2}	ρ_{liq}	$\delta\rho_{liq}$	ρ_{vap}	$\delta\rho_{vap}$	Δh_v^{res}	$\delta\Delta h_v^{res}$
K	MPa	MPa	mol/mol	mol/mol	mol/mol	mol/l	mol/l	mol/l	mol/l	kJ/mol	kJ/mol
83.15	0.196	0.002	0.00	0.000	0.000	27.899	0.005	0.302	0.003	5.401	0.001
83.15	1.27	0.01	0.03	0.812	0.002	28.111	0.005	1.952	0.008	5.194	0.002
83.15	1.98	0.01	0.05	0.866	0.001	28.255	0.005	3.098	0.011	5.024	0.002
83.15	3.05	0.01	0.08	0.898	0.001	28.461	0.005	4.897	0.018	4.761	0.002
83.15	3.76	0.02	0.10	0.903	0.001	28.589	0.007	6.158	0.032	4.579	0.003
83.15	4.63	0.02	0.12	0.910	0.001	28.758	0.005	7.748	0.034	4.364	0.003
83.15	5.96	0.03	0.16	0.910	0.001	29.013	0.007	10.312	0.052	4.033	0.004
83.15	7.06	0.04	0.19	0.906	0.001	29.211	0.016	12.501	0.071	3.76	0.01
83.15	9.18	0.07	0.24	0.890	0.002	29.595	0.026	16.742	0.120	3.26	0.01
83.15	14.8	0.3	0.40	0.815	0.005	30.624	0.085	25.770	0.452	1.89	0.02
100	0.792	0.003	0.00	0.000	0.000	24.644	0.008	1.143	0.004	4.552	0.002
100	1.815	0.005	0.03	0.485	0.002	24.760	0.009	2.522	0.007	4.409	0.003
100	2.47	0.01	0.05	0.584	0.002	24.829	0.009	3.447	0.008	4.261	0.003
100	3.48	0.01	0.08	0.666	0.001	24.913	0.008	4.880	0.014	4.029	0.003
100	4.12	0.01	0.10	0.690	0.002	24.976	0.008	5.854	0.016	3.863	0.004
100	4.84	0.02	0.12	0.711	0.002	24.999	0.009	6.945	0.023	3.67	0.01
100	5.98	0.02	0.16	0.728	0.002	25.075	0.011	8.712	0.031	3.37	0.01
100	6.88	0.03	0.19	0.731	0.002	25.081	0.025	10.184	0.041	3.11	0.01
100	8.44	0.04	0.24	0.708	0.003	25.123	0.033	13.119	0.068	2.59	0.01
100	10.53	0.12	0.33	0.579	0.007	24.934	0.101	19.297	0.212	1.36	0.03
110.3	1.515	0.004	0.00	0.000	0.000	22.207	0.028	2.251	0.006	3.809	0.004
110.3	2.44	0.01	0.03	0.280	0.001	22.189	0.031	3.481	0.009	3.66	0.01
110.3	3.03	0.01	0.05	0.375	0.002	22.174	0.028	4.300	0.011	3.52	0.01
110.3	3.94	0.01	0.08	0.455	0.002	22.163	0.021	5.621	0.016	3.29	0.01
110.3	4.46	0.01	0.10	0.488	0.002	22.076	0.022	6.379	0.018	3.13	0.01
110.3	5.16	0.02	0.12	0.511	0.002	22.048	0.019	7.503	0.023	2.91	0.01
110.3	6.06	0.02	0.16	0.543	0.002	21.904	0.014	8.847	0.036	2.64	0.01
110.3	6.80	0.03	0.19	0.536	0.003	21.758	0.057	10.331	0.045	2.32	0.01
110.3	8.00	0.04	0.24	0.509	0.006	21.474	0.042	13.152	0.071	1.71	0.04

5.1.2 Hydrogen + argon

Table S4: Homogeneous density data from molecular simulation for the equimolar mixture H_2 + Ar using the present as well as the H_2 force field of Marx and Nielaba[S1]. Statistical uncertainties are denoted by δ.

T	p	$\rho_{\mathrm{H2,present}}$	$\delta\rho_{\mathrm{H2,present}}$	$\rho_{\mathrm{H2,Marx}}$	$\delta\rho_{\mathrm{H2,Marx}}$
K	MPa	mol/l	mol/l	mol/l	mol/l
170.5	0.210	0.1484	0.0001	0.1484	0.0001
170.5	0.403	0.2859	0.0001	0.2860	0.0001
170.5	0.606	0.4304	0.0001	0.4307	0.0001
170.5	1.016	0.7252	0.0001	0.7262	0.0001
170.5	1.230	0.8798	0.0001	0.8810	0.0001
231.7	1.226	0.6372	0.0001	0.6377	0.0001
231.7	1.520	0.7901	0.0001	0.7909	0.0001
231.7	2.047	1.0643	0.0001	1.0658	0.0001
231.7	2.564	1.3332	0.0001	1.3356	0.0001
231.7	2.959	1.5388	0.0001	1.5420	0.0001
231.7	3.587	1.8657	0.0002	1.8703	0.0001
231.7	4.114	2.1398	0.0002	2.1460	0.0002
231.7	5.005	2.6043	0.0003	2.6129	0.0003
292.6	5.583	2.2578	0.0002	2.2645	0.0002
292.6	7.427	2.9849	0.0003	2.9961	0.0002
292.6	8.977	3.5882	0.0004	3.6040	0.0003

Table S5: Vapor-liquid equilibrium data from molecular simulation for H_2 + Ar using the present H_2 force field. Statistical uncertainties are denoted by δ.

T	p	δp	x_{H2}	y_{H2}	δy_{H2}	ρ_{liq}	$\delta\rho_{liq}$	ρ_{vap}	$\delta\rho_{vap}$	Δh_v^{res}	$\delta\Delta h_v^{res}$
K	MPa	MPa	mol/mol	mol/mol	mol/mol	mol/l	mol/l	mol/l	mol/l	kJ/mol	kJ/mol
85.8	0.090	0.001	0.00	0.000	0.000	35.147	0.003	0.130	0.001	6.452	0.001
85.8	3.03	0.01	0.03	0.953	0.001	35.350	0.003	4.32	0.02	6.116	0.001
85.8	5.16	0.03	0.05	0.960	0.001	35.505	0.004	7.31	0.04	5.871	0.002
85.8	8.42	0.06	0.08	0.957	0.001	35.736	0.006	11.66	0.08	5.511	0.003
85.8	10.71	0.08	0.10	0.951	0.001	35.909	0.008	14.5	0.1	5.273	0.004
85.8	13.5	0.1	0.12	0.946	0.001	36.11	0.01	17.6	0.1	5.00	0.01
85.8	18.0	0.2	0.16	0.933	0.002	36.45	0.02	21.8	0.3	4.61	0.01
85.8	21.4	0.3	0.19	0.924	0.002	36.70	0.03	24.4	0.4	4.31	0.01
85.8	28.3	0.8	0.24	0.896	0.002	37.24	0.07	28.8	0.8	3.75	0.02
85.8	34.0	0.7	0.30	0.890	0.003	37.69	0.06	31.2	0.6	3.32	0.02
100	0.331	0.002	0.00	0.000	0.000	32.837	0.005	0.428	0.003	5.997	0.001
100	2.90	0.01	0.03	0.837	0.001	32.977	0.005	3.62	0.01	5.732	0.002
100	4.61	0.02	0.05	0.871	0.001	33.071	0.005	5.72	0.02	5.514	0.003
100	7.22	0.03	0.08	0.888	0.001	33.219	0.007	8.83	0.04	5.192	0.003
100	8.91	0.05	0.10	0.891	0.001	33.306	0.009	10.76	0.06	4.983	0.004
100	10.86	0.07	0.12	0.886	0.001	33.39	0.01	12.92	0.08	4.73	0.01
100	14.0	0.1	0.16	0.876	0.002	33.59	0.02	16.2	0.1	4.35	0.01
100	16.1	0.2	0.19	0.870	0.002	33.63	0.02	18.1	0.2	4.07	0.01
100	20.4	0.3	0.24	0.847	0.003	33.85	0.05	21.7	0.4	3.53	0.02
100	27	2	0.33	0.807	0.004	34.1	0.3	26	2	2.71	0.04
120	1.220	0.003	0.00	0.000	0.000	29.098	0.007	1.481	0.004	5.106	0.002
120	3.25	0.01	0.03	0.520	0.002	29.126	0.008	3.734	0.009	4.910	0.004
120	4.56	0.01	0.05	0.607	0.002	29.099	0.009	5.20	0.01	4.713	0.005
120	6.47	0.02	0.08	0.669	0.002	29.08	0.01	7.28	0.02	4.42	0.01
120	7.63	0.03	0.10	0.692	0.002	29.03	0.01	8.51	0.03	4.24	0.01
120	9.01	0.04	0.12	0.701	0.003	28.96	0.02	10.03	0.05	3.99	0.01
120	10.92	0.06	0.16	0.705	0.002	28.82	0.02	12.05	0.06	3.63	0.01
120	13.0	0.1	0.19	0.691	0.003	28.94	0.06	14.4	0.1	3.27	0.01
120	15.6	0.2	0.24	0.664	0.007	28.63	0.09	17.3	0.2	2.66	0.04

Table S6: Vapor-liquid equilibrium data from molecular simulation for H_2 + Ar using the H_2 force field of Marx and Nielaba[S1]. Statistical uncertainties are denoted by δ.

T	p	δp	x_{H2}	y_{H2}	δy_{H2}	ρ_{liq}	$\delta\rho_{liq}$	ρ_{vap}	$\delta\rho_{vap}$	Δh_v^{res}	$\delta\Delta h_v^{res}$
K	MPa	MPa	mol/mol	mol/mol	mol/mol	mol/l	mol/l	mol/l	mol/l	kJ/mol	kJ/mol
85.8	0.088	0.001	0.00	0.000	0.000	35.147	0.005	0.127	0.002	6.454	0.001
85.8	2.599	0.01	0.03	0.951	0.001	35.386	0.005	3.88	0.02	6.072	0.001
85.8	4.421	0.03	0.05	0.962	0.001	35.568	0.005	6.83	0.04	5.787	0.002
85.8	7.624	0.06	0.08	0.960	0.001	35.868	0.006	12.29	0.09	5.320	0.003
85.8	9.686	0.08	0.10	0.958	0.001	36.061	0.008	15.7	0.1	5.034	0.004
85.8	13.202	0.12	0.12	0.946	0.001	36.38	0.01	21.0	0.2	4.64	0.01
85.8	19.116	0.37	0.16	0.928	0.002	36.93	0.03	27.3	0.5	4.13	0.01
85.8	25.644	1.44	0.19	0.916	0.003	37.5	0.1	32	2	3.77	0.03
100	0.331	0.002	0.00	0.000	0.000	32.837	0.005	0.428	0.003	5.997	0.001
100	2.56	0.01	0.03	0.829	0.001	32.997	0.005	3.27	0.01	5.710	0.002
100	4.09	0.02	0.05	0.874	0.001	33.131	0.005	5.31	0.02	5.477	0.002
100	6.46	0.03	0.08	0.893	0.001	33.315	0.006	8.54	0.04	5.112	0.003
100	8.03	0.04	0.10	0.896	0.001	33.438	0.007	10.68	0.05	4.873	0.003
100	10.18	0.06	0.12	0.891	0.001	33.628	0.009	13.64	0.08	4.56	0.01
100	13.2	0.1	0.16	0.884	0.002	33.87	0.01	17.5	0.1	4.15	0.01
100	16.2	0.2	0.19	0.871	0.003	34.13	0.02	20.8	0.2	3.78	0.01
100	21.1	0.4	0.24	0.851	0.004	34.57	0.05	25.2	0.4	3.23	0.02
100	29	1	0.33	0.825	0.004	35.3	0.2	30	1	2.49	0.03
120	1.220	0.003	0.00	0.000	0.000	29.098	0.007	1.481	0.004	5.106	0.002
120	3.10	0.01	0.03	0.507	0.002	29.156	0.008	3.599	0.008	4.904	0.003
120	4.29	0.01	0.05	0.607	0.002	29.174	0.009	4.96	0.01	4.722	0.004
120	6.06	0.02	0.08	0.670	0.002	29.18	0.01	7.03	0.02	4.41	0.01
120	7.22	0.03	0.10	0.696	0.002	29.180	0.009	8.36	0.03	4.21	0.01
120	8.66	0.04	0.12	0.705	0.002	29.21	0.02	10.12	0.05	3.95	0.01
120	10.55	0.05	0.16	0.712	0.002	29.18	0.01	12.39	0.06	3.57	0.01
120	12.12	0.09	0.19	0.708	0.003	29.17	0.05	14.3	0.1	3.26	0.01
120	14.3	0.1	0.24	0.688	0.005	28.90	0.05	17.0	0.1	2.69	0.02

5.1.3 Nitrogen + oxygen

Table S7: Homogeneous density data from molecular simulation for the equimolar mixture N_2 + O_2. Statistical uncertainties are denoted by δ.

T	p	ρ	$\delta\rho$
K	MPa	mol/l	mol/l
142.24	4.373	7.71	0.03
142.25	3.612	4.702	0.002
142.25	3.889	5.452	0.005
142.25	4.494	9.3	0.1
142.25	4.586	12.1	0.2
142.25	4.735	15.5	0.1
142.25	5.084	17.40	0.05
142.26	4.157	6.43	0.01
293.15	3.448	1.4324	0.0001
293.15	3.469	1.4413	0.0001
293.15	3.777	1.5705	0.0001
293.15	3.805	1.5822	0.0001
293.15	4.166	1.7342	0.0002
293.15	4.194	1.7458	0.0002
293.15	4.686	1.9534	0.0002
293.15	4.702	1.9602	0.0002
293.15	5.254	2.1924	0.0002
293.15	5.257	2.1934	0.0003
293.15	5.303	2.2135	0.0002

Table S8: Vapor-liquid equilibrium data from molecular simulation for N_2 + O_2. Statistical uncertainties are denoted by δ.

T	p	δp	x_{N2}	y_{N2}	δy_{N2}	ρ_{liq}	$\delta\rho_{liq}$	ρ_{vap}	$\delta\rho_{vap}$	Δh_v^{res}	$\delta\Delta h_v^{res}$
K	MPa	MPa	mol/mol	mol/mol	mol/mol	mol/l	mol/l	mol/l	mol/l	kJ/mol	kJ/mol
80	0.040	0.001	0.05	0.24	0.01	36.844	0.005	0.061	0.002	7.092	0.001
80	0.044	0.001	0.10	0.38	0.01	36.338	0.004	0.068	0.002	7.003	0.001
80	0.057	0.002	0.20	0.57	0.01	35.333	0.005	0.088	0.003	6.823	0.001
80	0.066	0.003	0.30	0.67	0.01	34.376	0.005	0.101	0.004	6.651	0.001
80	0.077	0.002	0.40	0.752	0.008	33.439	0.004	0.119	0.004	6.479	0.001
80	0.095	0.002	0.50	0.820	0.005	32.556	0.004	0.148	0.003	6.310	0.001
80	0.101	0.002	0.60	0.863	0.004	31.685	0.005	0.158	0.003	6.151	0.001
80	0.108	0.002	0.70	0.905	0.003	30.826	0.005	0.168	0.004	5.991	0.001
80	0.117	0.002	0.80	0.941	0.001	30.002	0.004	0.183	0.003	5.834	0.001
80	0.129	0.002	0.90	0.973	0.001	29.222	0.005	0.204	0.003	5.682	0.001
105	0.427	0.002	0.05	0.131	0.001	32.772	0.006	0.534	0.003	6.224	0.001
105	0.459	0.002	0.10	0.236	0.002	32.234	0.005	0.577	0.003	6.118	0.001
105	0.531	0.003	0.20	0.403	0.003	31.161	0.006	0.677	0.003	5.898	0.001
105	0.608	0.002	0.30	0.524	0.002	30.169	0.006	0.787	0.003	5.688	0.001
105	0.688	0.003	0.40	0.626	0.002	29.172	0.007	0.906	0.003	5.472	0.002
105	0.812	0.003	0.60	0.777	0.001	27.238	0.006	1.098	0.004	5.064	0.002
105	0.955	0.003	0.80	0.898	0.001	25.380	0.007	1.333	0.004	4.649	0.002
105	1.031	0.004	0.90	0.951	0.001	24.46	0.01	1.469	0.005	4.436	0.003
120	1.108	0.003	0.05	0.099	0.001	29.907	0.008	1.324	0.004	5.494	0.002
120	1.194	0.005	0.10	0.190	0.001	29.36	0.01	1.448	0.005	5.362	0.003
120	1.340	0.003	0.20	0.339	0.001	28.221	0.009	1.666	0.004	5.099	0.003
120	1.480	0.004	0.30	0.458	0.002	27.12	0.01	1.887	0.005	4.842	0.003
120	1.632	0.004	0.40	0.560	0.002	26.02	0.01	2.144	0.006	4.571	0.004
120	1.75	0.01	0.50	0.646	0.002	24.92	0.02	2.354	0.007	4.318	0.004
120	1.90	0.01	0.60	0.724	0.001	23.81	0.02	2.636	0.007	4.04	0.01
120	2.05	0.01	0.70	0.797	0.001	22.72	0.01	2.942	0.007	3.757	0.005
120	2.19	0.01	0.80	0.868	0.001	21.55	0.02	3.27	0.01	3.46	0.01
120	2.35	0.01	0.90	0.936	0.001	20.34	0.02	3.661	0.009	3.14	0.01

5.1.4 Nitrogen + argon

Table S9: Homogeneous density data from molecular simulation for the equimolar mixture N_2 + Ar. Statistical uncertainties are denoted by δ.

T	p	ρ	$\delta\rho$	T	p	ρ	$\delta\rho$
K	MPa	mol/l	mol/l	K	MPa	mol/l	mol/l
93.94	1.523	29.738	0.003	273.15	0.205	0.0903	0.0001
93.94	2.834	29.884	0.004	273.15	0.243	0.1074	0.0001
93.94	3.091	29.917	0.003	273.15	0.326	0.1438	0.0001
93.94	4.339	30.049	0.003	273.15	0.387	0.1709	0.0001
93.94	5.597	30.174	0.003	273.15	0.518	0.2288	0.0001
93.94	8.416	30.457	0.003	273.15	0.615	0.2720	0.0001
93.94	15.741	31.090	0.003	273.15	0.822	0.3642	0.0001
93.94	22.334	31.596	0.003	273.15	0.977	0.4330	0.0001
93.94	22.486	31.602	0.002	273.15	1.305	0.5797	0.0001
				273.15	1.549	0.6890	0.0001
203.19	0.311	0.1855	0.0001	273.15	2.068	0.9224	0.0001
203.19	0.356	0.2124	0.0001	273.15	2.452	1.0963	0.0001
203.19	0.493	0.2954	0.0001	273.15	3.267	1.4671	0.0001
203.19	0.564	0.3382	0.0001	273.15	3.871	1.7433	0.0002
203.19	0.780	0.4705	0.0001	273.15	5.149	2.3324	0.0002
203.19	0.892	0.5390	0.0001	273.15	6.096	2.7712	0.0003
203.19	1.230	0.7493	0.0001	273.15	8.101	3.7074	0.0005
203.19	1.403	0.8578	0.0001	273.15	9.595	4.4034	0.0006
203.19	1.927	1.1928	0.0001	273.15	12.809	5.8892	0.0009
203.19	2.193	1.3654	0.0002	273.15	15.269	6.998	0.001
203.19	2.990	1.8980	0.0003	273.15	20.881	9.359	0.002
203.19	3.391	2.1726	0.0003	273.15	25.604	11.119	0.002
203.19	4.579	3.0180	0.0005	273.15	38.425	14.868	0.003
203.19	5.170	3.4552	0.0006	273.15	52.108	17.662	0.003
203.19	6.899	4.798	0.001				
203.19	7.756	5.495	0.001				
203.19	10.295	7.633	0.002				
203.19	11.610	8.751	0.003				
203.19	16.054	12.187	0.005				
203.19	19.458	14.280	0.005				
203.19	33.731	19.421	0.003				
203.19	51.893	22.704	0.003				

Table S10: Vapor-liquid equilibrium data from molecular simulation for N_2 + Ar. Statistical uncertainties are denoted by δ.

T	p	δp	x_{N2}	y_{N2}	δy_{N2}	ρ_{liq}	$\delta\rho_{liq}$	ρ_{vap}	$\delta\rho_{vap}$	Δh_v^{res}	$\delta\Delta h_v^{res}$
K	MPa	MPa	mol/mol	mol/mol	mol/mol	mol/l	mol/l	mol/l	mol/l	kJ/mol	kJ/mol
90.49	0.146	0.002	0.00	0.000	0.000	34.397	0.005	0.202	0.002	6.311	0.001
90.49	0.195	0.001	0.20	0.404	0.004	32.602	0.006	0.274	0.002	6.034	0.001
90.49	0.246	0.002	0.40	0.627	0.003	30.949	0.006	0.349	0.002	5.776	0.001
90.49	0.290	0.002	0.60	0.781	0.002	29.397	0.006	0.417	0.003	5.531	0.001
90.49	0.339	0.002	0.80	0.901	0.001	27.950	0.006	0.495	0.003	5.298	0.001
90.49	0.381	0.002	1.00	1.000	0.000	26.556	0.006	0.563	0.003	5.072	0.001
109.99	0.673	0.003	0.00	0.000	0.000	31.061	0.006	0.832	0.004	5.600	0.001
109.99	0.838	0.002	0.20	0.331	0.002	29.164	0.007	1.068	0.003	5.247	0.002
109.99	0.967	0.003	0.35	0.508	0.002	27.827	0.008	1.265	0.004	4.985	0.002
109.99	1.156	0.003	0.60	0.730	0.001	25.645	0.009	1.576	0.005	4.557	0.003
109.99	1.318	0.004	0.80	0.873	0.001	23.97	0.01	1.868	0.005	4.208	0.003
109.99	1.477	0.005	1.00	1.000	0.000	22.29	0.01	2.179	0.007	3.847	0.004
122.89	1.421	0.005	0.00	0.000	0.000	28.48	0.01	1.725	0.006	4.941	0.003
122.89	1.708	0.005	0.20	0.296	0.001	26.43	0.01	2.181	0.006	4.499	0.004
122.89	1.993	0.005	0.40	0.515	0.001	24.42	0.01	2.697	0.006	4.042	0.005
122.89	2.27	0.01	0.60	0.691	0.001	22.36	0.02	3.269	0.008	3.559	0.007
122.89	2.58	0.01	0.80	0.851	0.001	20.22	0.03	4.07	0.01	3.00	0.01
122.89	2.93	0.01	1.00	1.000	0.000	17.66	0.05	5.35	0.01	2.25	0.02

5.1.5 Argon + oxygen

Table S11: Homogeneous density data from molecular simulation for the equimolar mixture Ar + O_2. Statistical uncertainties are denoted by δ.

T	p	ρ	$\delta\rho$
K	MPa	mol/l	mol/l
298.1	3.040	1.2470	0.0001
298.1	3.546	1.4583	0.0001
298.1	4.053	1.6708	0.0002
298.1	4.560	1.8840	0.0002
298.1	5.066	2.0982	0.0002
298.1	5.573	2.3126	0.0002
298.1	6.080	2.5278	0.0003
298.1	6.586	2.7443	0.0003
298.1	7.093	2.9606	0.0004
298.1	7.599	3.1782	0.0004
298.1	8.106	3.3958	0.0004
298.1	8.613	3.6135	0.0005
298.1	9.119	3.8317	0.0005
298.1	9.626	4.0497	0.0006
298.1	10.133	4.2678	0.0005
298.1	10.639	4.4867	0.0007
298.1	11.146	4.7060	0.0007
298.1	11.652	4.9253	0.0008
298.1	12.159	5.1429	0.0009
298.1	12.666	5.3604	0.0009

Table S12: Vapor-liquid equilibrium data from molecular simulation for Ar + O_2. Statistical uncertainties are denoted by δ.

T	p	δp	x_{Ar}	y_{Ar}	δy_{Ar}	ρ_{liq}	$\delta\rho_{\mathrm{liq}}$	ρ_{vap}	$\delta\rho_{\mathrm{vap}}$	$\Delta h_{\mathrm{v}}^{\mathrm{res}}$	$\delta\Delta h_{\mathrm{v}}^{\mathrm{res}}$
K	MPa	MPa	mol/mol	mol/mol	mol/mol	mol/l	mol/l	mol/l	mol/l	kJ/mol	kJ/mol
90	0.102	0.002	0.000	0.000	0.000	35.805	0.005	0.140	0.002	6.877	0.001
90	0.113	0.001	0.230	0.295	0.004	35.505	0.005	0.156	0.002	6.728	0.001
90	0.118	0.001	0.442	0.516	0.005	35.217	0.005	0.163	0.002	6.604	0.001
90	0.128	0.001	0.650	0.710	0.004	34.934	0.005	0.177	0.002	6.489	0.001
90	0.135	0.001	0.834	0.867	0.002	34.690	0.005	0.187	0.002	6.399	0.001
90	0.141	0.002	1.000	1.000	0.000	34.479	0.004	0.196	0.002	6.326	0.001
104.51	0.369	0.003	0.000	0.000	0.000	33.388	0.005	0.459	0.003	6.353	0.001
104.51	0.387	0.002	0.146	0.178	0.001	33.195	0.006	0.482	0.002	6.262	0.001
104.51	0.417	0.002	0.413	0.466	0.002	32.829	0.006	0.523	0.002	6.105	0.001
104.51	0.437	0.002	0.608	0.653	0.002	32.569	0.007	0.550	0.002	6.002	0.001
104.51	0.451	0.003	0.750	0.781	0.002	32.381	0.006	0.569	0.003	5.933	0.001
104.51	0.471	0.002	1.000	1.000	0.000	32.049	0.006	0.595	0.003	5.824	0.001
120.02	1.051	0.003	0.000	0.000	0.000	30.498	0.009	1.246	0.004	5.617	0.002
120.02	1.078	0.003	0.159	0.179	0.001	30.263	0.007	1.281	0.004	5.523	0.002
120.02	1.123	0.003	0.380	0.413	0.001	29.951	0.009	1.342	0.004	5.397	0.002
120.02	1.160	0.003	0.565	0.594	0.002	29.684	0.006	1.396	0.003	5.297	0.002
120.02	1.191	0.003	0.773	0.790	0.001	29.397	0.008	1.438	0.003	5.201	0.002
120.02	1.222	0.004	1.000	1.000	0.000	29.097	0.009	1.483	0.005	5.106	0.002

5.1.6 Nitrogen + water

Table S13: Vapor-liquid equilibrium data from molecular simulation for N_2 + H_2O. Statistical uncertainties are denoted by δ.

T	p	δp	x_{N2}	y_{N2}	δy_{N2}	ρ_{liq}	$\delta\rho_{liq}$	ρ_{vap}	$\delta\rho_{vap}$	Δh_v^{res}	$\delta\Delta h_v^{res}$
K	MPa	MPa	mol/mol	mol/mol	mol/mol	mol/l	mol/l	mol/l	mol/l	kJ/mol	kJ/mol
473.15	6.50	0.07	0.001	0.822	0.007	47.722	0.009	1.66	0.02	40.54	0.01
473.15	12.0	0.2	0.002	0.92	0.01	47.88	0.01	2.91	0.06	40.945	0.006
473.15	18.9	0.2	0.003	0.939	0.003	48.09	0.01	4.45	0.04	40.69	0.01
473.15	26.3	0.2	0.004	0.950	0.002	48.32	0.01	5.93	0.05	40.59	0.01
473.15	34.4	0.4	0.005	0.967	0.002	48.57	0.02	7.38	0.09	40.59	0.01
573.15	12.3	0.1	0.004	0.388	0.003	38.85	0.02	3.23	0.03	29.62	0.05
573.15	15.7	0.2	0.006	0.505	0.004	39.05	0.02	3.80	0.04	30.79	0.05
573.15	23.6	0.2	0.010	0.614	0.004	39.45	0.02	5.29	0.05	31.29	0.06
573.15	31.6	0.6	0.014	0.730	0.005	39.80	0.04	6.4	0.1	32.64	0.04
573.15	41.8	0.6	0.018	0.763	0.004	40.27	0.04	7.9	0.1	32.62	0.05

5.1.7 Hydrogen + water

Table S14: Vapor-liquid equilibrium data from molecular simulation for H_2 + H_2O using the present H_2 force field. Statistical uncertainties are denoted by δ.

T	p	δp	x_{H2}	y_{H2}	δy_{H2}	ρ_{liq}	$\delta\rho_{liq}$	ρ_{vap}	$\delta\rho_{vap}$	Δh_v^{res}	$\delta\Delta h_v^{res}$
K	MPa	MPa	mol/mol	mol/mol	mol/mol	mol/l	mol/l	mol/l	mol/l	kJ/mol	kJ/mol
423	6.09	0.04	0.001	0.938	0.005	50.79	0.01	1.69	0.01	43.735	0.008
423	11.92	0.07	0.002	0.979	0.003	50.96	0.01	3.20	0.02	43.827	0.004
423	18.29	0.09	0.003	0.979	0.002	51.14	0.01	4.77	0.02	43.788	0.006
477.59	4.63	0.09	0.001	0.77	0.01	47.33	0.01	1.18	0.02	40.42	0.02
477.59	8.63	0.08	0.002	0.859	0.006	47.49	0.01	2.14	0.02	40.61	0.01
477.59	12.47	0.10	0.003	0.904	0.005	47.63	0.01	3.02	0.02	40.76	0.01

Table S15: Vapor-liquid equilibrium data from molecular simulation for H_2 + H_2O using the H_2 force field of Marx and Nielaba[S1]. Statistical uncertainties are denoted by δ.

T	p	δp	x_{H2}	y_{H2}	δy_{H2}	ρ_{liq}	$\delta\rho_{liq}$	ρ_{vap}	$\delta\rho_{vap}$	Δh_v^{res}	$\delta\Delta h_v^{res}$
K	MPa	MPa	mol/mol	mol/mol	mol/mol	mol/l	mol/l	mol/l	mol/l	kJ/mol	kJ/mol
423	5.71	0.03	0.001	0.948	0.004	50.793	0.009	1.59	0.01	43.756	0.007
423	11.11	0.05	0.002	0.997	0.002	50.949	0.009	3.01	0.01	43.804	0.003
423	17.11	0.09	0.003	0.985	0.001	51.12	0.01	4.52	0.02	43.736	0.005
477.59	4.49	0.07	0.001	0.76	0.01	47.37	0.01	1.15	0.02	40.35	0.01
477.59	8.07	0.07	0.002	0.863	0.007	47.50	0.01	2.01	0.02	40.64	0.01
477.59	11.8	0.1	0.003	0.908	0.006	47.63	0.01	2.87	0.02	40.764	0.009

Table S16: Henry's law constant data from molecular simulation for H_2 (present as well as Marx and Nielaba force field[S1]), N_2, O_2 and Ar in H_2O. Statistical uncertainties are denoted by δ.

T	$H_{\mathrm{H2,present}}$	$\delta H_{\mathrm{H2,present}}$	$H_{\mathrm{H2,Marx}}$	$\delta H_{\mathrm{H2,Marx}}$	H_{N2}	δH_{N2}	H_{O2}	δH_{O2}	H_{Ar}	δH_{Ar}
K	GPa	GPa	GPa	GPa	GPa	GPa	GPa	GPa	GPa	GPa
280	5.68	0.09	6.29	0.07	6.5	0.2	3.30	0.07	2.89	0.06
290	6.27	0.08	6.88	0.07	7.6	0.2	4.02	0.09	3.49	0.07
300	6.9	0.1	7.40	0.08	8.8	0.2	4.65	0.08	4.10	0.07
310	7.51	0.08	7.79	0.07	10.0	0.2	5.34	0.09	4.70	0.08
323	7.69	0.08	7.87	0.05	11.0	0.2	5.93	0.08	5.26	0.07
332	7.81	0.07	7.86	0.05	11.1	0.2	6.18	0.08	5.51	0.07
340	7.83	0.07	7.82	0.05	11.4	0.2	6.38	0.07	5.70	0.07
350	7.81	0.06	7.69	0.04	11.5	0.2	6.58	0.07	5.89	0.06
360	7.74	0.05	7.51	0.04	11.4	0.1	6.63	0.06	5.94	0.05
370	7.46	0.04	7.18	0.03	10.9	0.1	6.52	0.06	5.88	0.05
385	7.05	0.04	6.75	0.03	10.35	0.09	6.34	0.04	5.75	0.04
400	6.64	0.03	6.26	0.02	9.65	0.08	6.06	0.04	5.51	0.04
425	5.65	0.03	5.33	0.02	8.13	0.06	5.34	0.03	4.89	0.03
450	4.67	0.02	4.39	0.01	6.92	0.04	4.54	0.02	4.17	0.02
475	3.82	0.01	3.59	0.01	5.43	0.03	3.73	0.02	3.45	0.01
500	3.04	0.01	2.87	0.01	4.18	0.02	3.00	0.01	2.78	0.01
525	2.37	0.01	2.25	0.01	3.16	0.02	2.36	0.01	2.20	0.01
550	1.82	0.01	1.74	0.01	2.31	0.01	1.80	0.01	1.69	0.01
575	1.37	0.01	1.316	0.005	1.62	0.01	1.35	0.01	1.27	0.01
600	0.984	0.005	0.955	0.004	1.12	0.01	0.964	0.004	0.914	0.004
625	0.697	0.004	0.681	0.004	0.764	0.004	0.678	0.004	0.647	0.003

5.2 Ternary mixtures

5.2.1 Nitrogen + oxygen + argon

Table S17: Homogeneous density data from molecular simulation for N_2 + O_2 + Ar at the composition of ambient air $x_{N2} = 0.781$, $x_{O2} = 0.210$ and $x_{Ar} = 0.009$ mol/mol. Statistical uncertainties are denoted by δ.

T	p	ρ	$\delta\rho$	T	p	ρ	$\delta\rho$
K	MPa	mol/l	mol/l	K	MPa	mol/l	mol/l
70	3.510	32.000	0.003	873.19	1.555	0.2131	0.0001
70	6.930	32.205	0.003	873.19	10.170	1.3496	0.0001
70	10.220	32.396	0.003	873.19	22.290	2.8309	0.0002
70	13.990	32.609	0.003	873.19	34.090	4.1506	0.0003
70	17.370	32.786	0.003	873.19	41.550	4.9292	0.0004
70	20.520	32.945	0.003	873.19	48.220	5.5925	0.0005
70	24.340	33.134	0.002	873.19	55.620	6.2927	0.0005
70	28.340	33.321	0.003	873.19	100.000	9.8648	0.0008
				873.19	150.000	12.9477	0.0009
473.15	2.473	0.6232	0.0001	873.19	200.000	15.388	0.001
473.15	5.069	1.2642	0.0001	873.19	250.000	17.396	0.001
473.15	10.004	2.4433	0.0002	873.19	300.000	19.094	0.001
473.15	14.620	3.4955	0.0003	873.19	350.000	20.566	0.001
473.15	20.540	4.7695	0.0005	873.19	400.000	21.861	0.001
473.15	26.450	5.9578	0.0007	873.19	450.000	23.020	0.001
473.15	33.910	7.3409	0.0008	873.19	500.000	24.066	0.001
473.15	40.890	8.525	0.001				
473.15	51.390	10.122	0.001	1500	100.000	6.4245	0.0005
473.15	61.860	11.527	0.001	1500	150.000	8.7916	0.0007
473.15	69.470	12.450	0.001	1500	200.000	10.8034	0.0009
473.15	100.000	15.497	0.002	1500	250.000	12.5428	0.0009
473.15	150.000	19.049	0.001	1500	300.000	14.076	0.001
473.15	200.000	21.606	0.001	1500	350.000	15.442	0.001
473.15	250.000	23.601	0.001	1500	400.000	16.674	0.001
473.15	300.000	25.235	0.001	1500	450.000	17.795	0.001
473.15	350.000	26.619	0.001	1500	500.000	18.824	0.001
473.15	400.000	27.821	0.001				
473.15	450.000	28.885	0.001				
473.15	500.000	29.838	0.001				

Table S18: Vapor-liquid equilibrium data from molecular simulation for N_2 + O_2 + Ar. Statistical uncertainties are denoted by δ.

T	p	δp	x_{N2}	x_{O2}	x_{Ar}	y_{N2}	δy_{N2}	y_{O2}	δy_{O2}	y_{Ar}	δy_{Ar}
K	MPa	MPa	mol/mol	mol/mol	mol/mol	mol/mol	mol/mol	mol/mol	mol/mol	mol/mol	mol/mol
84.7	0.138	0.003	0.460	0.450	0.090	0.753	0.001	0.193	0.001	0.054	0.001
84.7	0.142	0.004	0.440	0.310	0.250	0.717	0.001	0.135	0.001	0.148	0.001
84.7	0.133	0.003	0.370	0.270	0.360	0.645	0.001	0.125	0.001	0.231	0.001
84.7	0.141	0.003	0.390	0.160	0.450	0.661	0.001	0.069	0.001	0.270	0.001
84.7	0.129	0.003	0.330	0.010	0.660	0.588	0.001	0.000	0.000	0.412	0.001
120	1.976	0.006	0.600	0.075	0.325	0.705	0.001	0.050	0.002	0.245	0.001
120	1.974	0.006	0.600	0.100	0.300	0.708	0.001	0.066	0.002	0.225	0.001
120	1.970	0.005	0.600	0.130	0.270	0.710	0.001	0.088	0.001	0.201	0.001
120	1.963	0.005	0.615	0.150	0.235	0.724	0.001	0.101	0.002	0.175	0.001
120	1.980	0.005	0.613	0.237	0.150	0.728	0.001	0.162	0.002	0.111	0.001
120	1.958	0.005	0.619	0.288	0.093	0.734	0.001	0.197	0.002	0.069	0.001

5.2.2 Hydrogen + nitrogen + argon

Table S19: Vapor-liquid equilibrium data from molecular simulation for H_2 + N_2 + Ar. Statistical uncertainties are denoted by δ.

T	p	δp	x_{H2}	x_{N2}	x_{Ar}	y_{H2}	δy_{H2}	y_{N2}	δy_{N2}	y_{Ar}	δy_{Ar}
K	MPa	MPa	mol/mol	mol/mol	mol/mol	mol/mol	mol/mol	mol/mol	mol/mol	mol/mol	mol/mol
100	2.04	0.01	0.027	0.626	0.347	0.613	0.002	0.303	0.002	0.084	0.003
100	2.04	0.01	0.029	0.780	0.191	0.574	0.002	0.379	0.002	0.048	0.003
100	2.07	0.01	0.031	0.909	0.060	0.543	0.002	0.442	0.002	0.015	0.003
100	2.09	0.01	0.031	0.825	0.144	0.573	0.002	0.391	0.002	0.035	0.003
100	2.12	0.01	0.032	0.850	0.118	0.569	0.002	0.402	0.002	0.029	0.003
100	3.03	0.01	0.036	0.206	0.758	0.074	0.002	0.800	0.001	0.126	0.002
100	3.05	0.01	0.037	0.265	0.698	0.097	0.002	0.781	0.001	0.122	0.002
100	3.01	0.01	0.046	0.617	0.337	0.227	0.002	0.709	0.002	0.064	0.002
100	3.03	0.01	0.047	0.619	0.334	0.226	0.002	0.711	0.002	0.062	0.002
100	3.11	0.01	0.052	0.751	0.197	0.279	0.002	0.682	0.002	0.038	0.003

5.3 Quaternary mixture

5.3.1 Nitrogen + oxygen + argon + water

Table S20: Homogeneous density data from molecular simulation for N_2 + O_2 + Ar + H_2O at a composition of $x_{N2} = 0.758$, $x_{O2} = 0.204$, $x_{Ar} = 0.009$ and $x_{H2O} = 0.029$ mol/mol (humid air). Statistical uncertainties are denoted by δ.

T	p	ρ	$\delta\rho$	T	p	ρ	$\delta\rho$
K	MPa	mol/l	mol/l	K	MPa	mol/l	mol/l
273.15	5	2.2933	0.0006	673	5	0.8762	0.0001
273.15	10	4.628	0.001	673	10	1.7168	0.0001
273.15	15	6.872	0.002	673	15	2.5224	0.0002
273.15	20	8.932	0.002	673	20	3.2939	0.0003
273.15	25	10.746	0.002	673	25	4.0319	0.0003
273.15	30	12.323	0.002	673	30	4.7390	0.0004
273.15	35	13.686	0.003	673	35	5.4154	0.0005
273.15	40	14.864	0.003	673	40	6.0622	0.0006
273.15	45	15.899	0.003	673	45	6.6821	0.0006
273.15	50	16.816	0.003	673	50	7.2748	0.0007
273.15	100	22.521	0.002	673	100	12.072	0.001
273.15	150	25.654	0.002	673	150	15.470	0.001
273.15	200	27.837	0.002	673	200	18.057	0.001
273.15	250	29.521	0.002	673	250	20.129	0.001
273.15	300	30.902	0.002	673	300	21.850	0.001
472.15	5	1.2515	0.0001	1500	5	0.3961	0.0001
472.15	10	2.4530	0.0002	1500	10	0.7827	0.0001
472.15	15	3.5990	0.0005	1500	15	1.1598	0.0001
472.15	20	4.6864	0.0005	1500	20	1.5281	0.0001
472.15	25	5.7141	0.0006	1500	25	1.8877	0.0001
472.15	30	6.6828	0.0008	1500	30	2.2391	0.0001
472.15	35	7.5958	0.0009	1500	35	2.5824	0.0002
472.15	40	8.4524	0.0009	1500	40	2.9178	0.0002
472.15	45	9.259	0.001	1500	45	3.2462	0.0002
472.15	50	10.020	0.001	1500	50	3.5675	0.0003
472.15	100	15.680	0.002	1500	100	6.4394	0.0006
472.15	150	19.285	0.002	1500	150	8.8192	0.0006
472.15	200	21.876	0.003	1500	200	10.8416	0.0007
472.15	250	23.897	0.002	1500	250	12.594	0.001
472.15	300	25.548	0.003	1500	300	14.138	0.001

Table S21: Homogeneous density data from molecular simulation for N_2 + O_2 + Ar + H_2O at a composition of $x_{N2} = 0.163$, $x_{O2} = 0.044$, $x_{Ar} = 0.002$ and $x_{H2O} = 0.791$ mol/mol (supercritical H_2O containing ≈ 0.2 mol/mol of air components). Statistical uncertainties are denoted by δ.

T	p	ρ	$\delta\rho$
K	MPa	mol/l	mol/l
672.95	33.3	9.53	0.01
672.95	52.2	15.74	0.01
672.95	80.9	21.92	0.01
672.95	118.6	26.78	0.01
672.95	172.6	31.21	0.01
672.95	214.2	33.61	0.01
672.95	233.0	34.54	0.01
672.95	249.3	35.26	0.01
672.95	279.5	36.51	0.01

References

(S1) Marx, D.; Nielaba, P. Path-integral Monte Carlo techniques for rotational motion in two dimensions: Quenched, annealed, and no-spin quantum-statistical averages. *Phys. Rev. A* **1992**, *45*, 8968–8971.

(S2) Fastovskii, V. G.; Petrovskii, Y. V. A study of the vapor-liquid equilibrium in the system oxygen-argon-nitrogen. *Zh. Fiz. Khim.* **1957**, *31*, 836–841.

(S3) Xiao, J.; Liu, K. Measurement and correlation of vapor - liquid equilibrium data in H2 - N2 - Ar system. *J. Chem. Eng. (China)* **1990**, *8*, 8–12.

(S4) Kunz, O.; Wagner, W. The GERG-2008 wide-range equation of state for natural gases and other mixtures: an expansion of GERG-2004. *J. Chem. Eng. Data* **2012**, *57*, 3032–3091.

(S5) Eubanks, L. S. Vapor-Liquid equilibria in the system Hydrogen-Nitrogen-Carbon monoxide. Ph.D. thesis, Rice University, 1957.

(S6) Akers, W. W.; Eubanks, L. S. Vapor-Liquid Equilibria in the System Hydrogen-Nitrogen-Carbon Monoxide. *Adv. Cryog. Eng.* **1960**, *3*, 275–293.

(S7) Streett, W. B.; Calado, J. C. G. Liquid-vapour equilibrium for hydrogen + nitrogen at temperatures from 63 to 110 K and pressures to 57 MPa. *J. Chem. Thermodyn.* **1978**, *10*, 1089–1100.

(S8) Calado, J. C. G.; Streett, W. B. Liquid-vapor equilibrium in the system H_2 + Ar at temperatures from 83 to 141 K and pressures to 52 MPa. *Fluid Phase Equilib.* **1979**, *2*, 275–282.

(S9) Ostronov, M. G.; Shatskaya, L. V.; Finyagina, R. A.; Brodskaya, L. F.; Zhirnova, N. A. Gas-Liquid Phase Equilibrium in the Argon-Hydrogen System at Intermediate Pressures. *Russ. J. Phys. Chem.* **1977**, *51*, 1407–1409.

(S10) Volk, H.; Halsey Jr., G. D. Solubility of hydrogen and deuterium in liquid argon. *J. Chem. Phys.* **1960**, *33*, 1132–1139.

(S11) Mullins, J. C.; Ziegler, W. T. Phase equilibria in the argon-helium and argon-hydrogen systems from 68 to 108 K and pressures to 120 atmospheres. *Adv. Cryog. Eng.* **1965**, *10*, 171–181.

(S12) International Association for the Properties of Water and Steam, *Guideline on the Henry's Constant and Vapor-Liquid Distribution Constant for Gases in H_2O and D_2O at High Temperatures*. 2004.

(S13) Fernández-Prini, R.; Alvarez, J. L.; Harvey, A. H. Henry's constants and vapor–liquid distribution constants for gaseous solutes in H_2O and D_2O at high temperatures. *J. Phys. Chem. Ref. Data* **2003**, *32*, 903–916.

(S14) Morris, D. R.; Yang, L.; Giraudeau, F.; Sun, X.; Steward, F. R. Henry's law constant for hydrogen in natural water and deuterium in heavy water. *Phys. Chem. Chem. Phys.* **2001**, *3*, 1043–1046.

(S15) Alvarez, J.; Fernández-Prini, R. A semiempirical procedure to describe the thermodynamics of dissolution of non-polar gases in water. *Fluid Phase Equilib.* **1991**, *66*, 309–326.

(S16) Rettich, T. R.; Battino, R.; Wilhelm, E. Solubility of gases in liquids. XVI. Henry's law coefficients for nitrogen in water at 5 to 50° C. *J. Solution Chem.* **1984**, *13*, 335–348.

(S17) Cosgrove, B. A.; Walkley, J. Solubilities of gases in H_2O and ^2H_2O. *J. Chromatogr. A* **1981**, *216*, 161–167.

(S18) Alvarez, J.; Crovetto, R.; Fernández-Prini, R. The dissolution of N_2 and of H_2 in water from room temperature to 640 K. *Ber. Bunsenges. Phys. Chem.* **1988**, *92*, 935–940.

(S19) Rettich, T. R.; Battino, R.; Wilhelm, E. Solubility of gases in liquids. 22. High-precision determination of Henry's law constants of oxygen in liquid water from T= 274 K to T= 328 K. *J. Chem. Thermodyn.* **2000**, *32*, 1145–1156.

(S20) Benson, B. B.; Krause, D.; Peterson, M. A. The solubility and isotopic fractionation of gases in dilute aqueous solution. I. Oxygen. *J. Solution Chem.* **1979**, *8*, 655–690.

(S21) Rettich, T. R.; Handa, Y. P.; Battino, R.; Wilhelm, E. Solubility of gases in liquids. 13. High-precision determination of Henry's constants for methane and ethane in liquid water at 275 to 328 K. *J. Phys. Chem.* **1981**, *85*, 3230–3237.

(S22) Cramer, S. D. The solubility of oxygen in brines from 0 to 300° C. *Ind. Eng. Chem. Process Des. Dev.* **1980**, *19*, 300–305.

(S23) Rettich, T. R.; Battino, R.; Wilhelm, E. Solubility of gases in liquids. 18. High-precision determination of Henry fugacities for argon in liquid water at 2 to 40° C. *J. Solution Chem.* **1992**, *21*, 987–1004.

(S24) Krause, D.; Benson, B. B. The solubility and isotopic fractionation of gases in dilute aqueous solution. IIa. Solubilities of the noble gases. *J. Solution Chem.* **1989**, *18*, 823–873.

(S25) Potter, R. W.; Clynne, M. A. The solubility of the noble gases He, Ne, Ar, Kr, and Xe in water up to the critical point. *J. Solution Chem.* **1978**, *7*, 837–844.

(S26) Crovetto, R.; Fernández-Prini, R.; Japas, M. L. Solubilities of inert gases and methane in H_2O and in D_2O in the temperature range of 300 to 600 K. *J. Chem. Phys.* **1982**, *76*, 1077–1086.